NEW TOOL DESIGN FOR MEASURING TOOL DISPLACEMENT IN MILLING

A Thesis

presented to

the Faculty of the Graduate School

at the University of Missouri-Columbia

In Partial Fulfillment

of the Requirements for the Degree

Master of Science

---

by

BRIAN MOONEY

Dr. Roger Fales, Thesis Supervisor

DECEMBER 2012

The undersigned, appointed by the dean of the Graduate School, have examined the thesis entitled

NEW TOOL DESIGN FOR MEASURING TOOL

DISPLACEMENT IN MILLING

presented by Brian Mooney,

a candidate for the degree of Master of Science,

and hereby certify that, in their opinion, it is worthy of acceptance.

Professor Roger Fales

Professor Yuyi Lin

Professor Stephen Montgomery-Smith

ACKNOWLEDGEMENTS

I would like to thank my advisor Dr. Roger Fales for his contribution to this research. His guidance and involvement throughout this research was vital to this work becoming a success. I would also like to thank Dr. Stephen Montgomery-Smith and Dr. Yuyi Lin for serving on my committee and their invaluable help throughout my graduate career.

Finally, I would like to thank my parents Richard and Kathleen Mooney, whose unwavering support and encouragement has made the completion of this thesis possible.

TABLE OF CONTENTS

LIST OF FIGURES

LIST OF TABLES

Abstract

The goal of this research is to validate the concept for a new tool design which can allow measurement of the tool displacement during a milling operation. Monitoring the tool displacement during a milling process allows the operator to identify when there is relative movement between the cutting tool and the workpiece. When the relative movement between the cutting tool and the workpiece becomes large enough, the displacements of the cutting tool become known as chatter. Chatter produces a dimensionally inaccurate cut, poor surface finish, tool breakage, and is the main obstacle in high speed milling. If the milling machine or operator were able to detect the smaller tool displacements leading up to chatter, then the milling operation can be altered to eliminate the onset of chatter.

There are many different chatter detection methods currently used in industry today. But most are intrusive in the milling process or else the detection method is delayed and chatter must occur for a short period of time before the system acknowledges that chatter is present. The new tool design is non-intrusive and will be able to detect the forewarning displacements in the cutting tool before the milling operation becomes unstable and begins to chatter.

Prior tool displacement measurement methods have been conducted by measuring the *x* and *y* displacements directly. The presence of the sensors surrounding the cutting tool leaves this method impractical for industrial use. The new tool design discussed in this research will allow for tool displacement measurement to be utilized in industry.

The concept behind this new tool design is to indirectly measure the tool's displacement in the x and *y* direction by attaching a thin disc perpendicular to the neck of the cutting tool. The disc will allow sensors to measure the angle of deflection in the neck of the cutting tool by measuring the resulting tilt in the disc. Measuring the disc's displacement rather than the actual tool's displacement allows for the sensors to be placed above the cutting tool and away from milling operations.

In this research, the concept behind the indirect measurement of the tool displacement was performed experimentally, and results were verified using alternative tool displacement techniques and finite element analysis. Validating the conceptual new tool design will promote future research to be conducted on this topic.

A modified version of the new tool design is also presented in this paper. The modified version is based on the same principle of indirectly measuring the cutting tool displacement, and is the ideal tool design for industrial use.

Chapter 1: Introduction

In this Chapter, the general concepts behind the milling process and chatter are discussed. Cutting tool deflection and chatter occurring during milling operations lead to a poor cut and damage to the cutting tool. This research first explains the problems of tool displacement in milling and the solutions currently used in industry to fix this major problem in milling. After establishing the current situation, an entirely new method to prevent tool displacement and chatter in milling is presented and validated by this research.

A review of the milling process can be found in Section 1.1. A background in the advantages in high speed milling can be found in Section 1.2. A background in chatter can be found in Section 1.3. The mathematical milling model can be found in Section 1.4. The motivation behind this research can be found in Section 1.5.

1.1: A Background in Milling

Milling is a machining process in which a rotating cutting tool uses the teeth or flutes on the tool's edges to remove material from a workpiece to achieve desired dimensions or surface finish. Milling can be categorized into three types of operation known as peripheral milling, face milling, and end milling [1, 2]. In peripheral milling, the milled surface is generated by teeth located on the periphery of the cutter body, and the axis of cutter rotation is generally in a plane parallel to the workpiece surface being machined. In face milling, the milled surface results from the action of cutting edges located on the periphery and face of the cutter with the axis of cutter rotation perpendicular to the workpiece surface being machined. For end milling, the milling surface is generated by the teeth located on both the periphery and the tip of the cutting tool with the axis of cutter rotation perpendicular to the workpiece [2].

These three milling types of operations can be further classified as up-milling, down-milling, or slot milling which refers to the feed direction of the workpiece. During up milling, the

feed rate is directed along the opposite direction as the rotation of the tool. During down milling, the feed rate is directed along the same direction as the rotation of the tool. The chip formation in down milling is opposite to that seen in up milling [3]. The difference between up-milling and down- milling can be observed in Figure 1. Slot milling is when the radial immersion of the cutting tool is greater than the cutting tool's diameter, which results in a combination of both up-milling and down-milling. Diagrams for up-milling, down milling, and slot milling process can be seen in Figure 1.

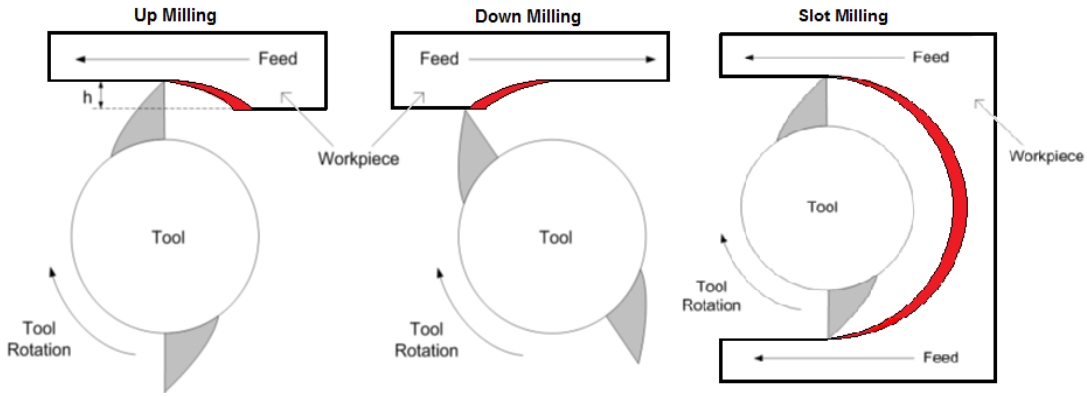

Figure 1: Diagram of an up milling, down milling, and slot milling process (shown from top looking down).The depth of cut, b, is into the paper. The radial immersion is represented by *h.* Slot milling is when the radial immersion, h, is greater than the diameter of the cutting tool.

1.2: A Background in the Advantages of High Speed Milling

Maximizing productivity is a primary goal in the machining process. For milling processes, this frequently translates into maximizing the material removal rate. The factors that determine the material removal rate are the feed rate, depth of cut, and radial immersion of the tool. Increasing these factors result in a higher material removal rate [4].

Improvements to spindles have been developed so that they could rotate at much higher speeds while retaining good stiffness, which is essential for maintaining the dimensional accuracy of the machined part [5]. Given its ability for high removal rates and low location error,

high speed milling is one of the most cost effective machining operations available [6]. However, to capture substantial cost savings typically requires taking full advantage of a machining center's capabilities and using accurate predictive analysis to avoid unstable oscillations [7]. Dynamic models provide the ability to predict surface accuracy and regions of stable cutting for a large combination of process parameters. Hence, the typical industrial trial and error results can be minimized and the selection of the optimum machining parameters can be implemented for best manufacturability and cost reduction [8].

1.3: A Background in Chatter

Chatter in milling is the relative movement of the cutting tool to the workpiece while performing a milling operation which results in a dimensionally inaccurate cut and poor surface finish. This machining vibration can be due to many factors. One factor for the occurrence of chatter in end milling is the chip formation which can be observed in Fig. 1. The red area represents the area that will be cut away in the current tooth path. For end milling, the tooth enters and exits the workpiece for each turn and creates an interrupted process since the tooth is not continually in contact with the workpiece. This becomes more prevalent in low radial immersion cuts since the cutting tooth and workpiece are out of cut for longer periods of time [10]. This inconsistency of the cutting forces between the cutting tool and the workpiece creates relative oscillations between the cutting tool and the work piece, and is the primary limiting factor of material removal rate [11].

Another factor for the presence of chatter during a milling operation is the regenerative effect. This regenerative effect is due to the fact that the current tooth pass of the cutting tool is cutting the surface of the previous tooth pass [12]. Therefore, the previous cut being inaccurate will lead to the current cut being inaccurate as well creating a continuous cycle of inaccurate cuts.

1.4: The Mathematical Milling Model

Milling is a process that has multiple cutting teeth, a rotating tool, multiple degrees-of freedom tool dynamics, and varying cutting forces and chip thicknesses [9]. The modeling of a milling operation is complex and actual results will vary between different tools, milling operations, and change over time due to tool wear.

1.4.1: Geometry of the Milling Model

Several models for describing the dynamic behavior of a milling process exist. The most common of the milling models assumes non-rotating restoring and damping forces and negligible mass imbalance [8] (see Figure 2). The workpiece is assumed to be rigid, and the tool is assumed to be flexible [5].

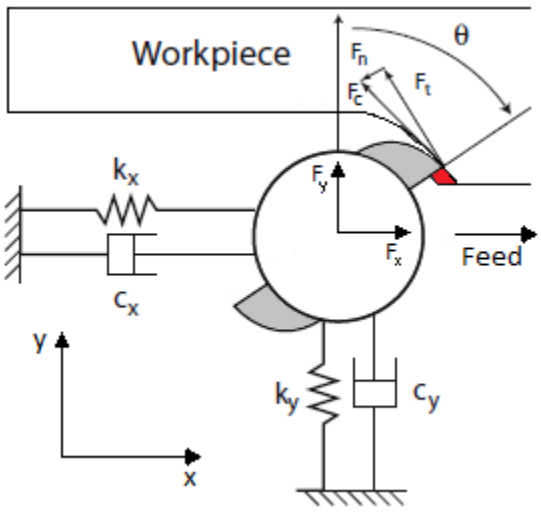

Figure 2: Schematic diagram of the mathematical milling model assuming non-rotating restoring and damping forces. The directional cutting forces are F_t and F_n for the forces in the tangential and normal directions. F_c is the term for the resultant cutting force.

The cutting forces are applied when one or more cutting teeth are engaged with the workpiece. The force acting on each cutting tooth is turned on and off as the cutting tooth enters and exits the workpiece. The path for each subsequent cutting tooth is trochoidal, but as

long as the feed rate is much smaller than the cutter radius, a circular arc is a reasonable approximation for the trochoidal path. The paths of subsequent teeth are represented by circles mutually shifted in the direction of feed rate per tooth [17]. For a circular tool path, the entry and exit angle of the cutting tooth is expressed as

$$\left.\begin{matrix}\theta_{in} = 0 \\ \theta_{out} = \cos^{-1}(1 - \frac{h}{r})\end{matrix}\right\} \text{Up-Milling} \quad (1)$$

$$\left.\begin{matrix}\theta_{in} = \pi - \cos^{-1}(1 - \frac{h}{r}) \\ \theta_{out} = \pi\end{matrix}\right\} \text{Down-Milling} \quad (2)$$

$$\left.\begin{matrix}\theta_{in} = 0 \\ \theta_{out} = \pi\end{matrix}\right\} \text{Slot Milling} \quad (3)$$

where *h* is the radial immersion and *r* is the cutting tool radius.

1.4.2: Chip Thickness Calculation

To determine the tangential and normal cutting forces, the instantaneous chip thickness must be determined. The instantaneous chip thickness, ω_p, on the P^{th} tooth can be approximated as

$$\omega_p(t) = hsin\theta_p(t) + [x(t) - x(t-\tau)]sin\theta_p(t) + [y(t) - y(t-\tau)]cos\theta_p(t) \quad (4)$$

where *h* is the feed per tooth, θ is the cutter rotation angle, $\tau = \frac{60}{N\Omega}$ is the time delay from the previous tooth pass, where *N* is the number of teeth and Ω is the spindle speed in rpm. $x(t)$ and $y(t)$ are the tool's current location along the *x* and *y* direction, and $x(t-\tau)$ and $y(t-\tau)$ was the tool's location along the *x* and *y* direction from the previous tooth pass [8, 14].

1.4.3: Cutting Forces in Milling

The cutting forces in milling are the product of the tool geometry, tool wear, cutting parameters, material selection, and surface finish. Since milling is an interrupted cutting process where the cutting tooth enters and exits the workpiece, a discontinuous expression is required to model the cutting forces. A tangential force F_t, and normal force F_n, are applied to the cutting tooth as the tooth is engaged in the workpiece. The tangential and normal forces are proportional to the cutting area and therefore are a function of chip geometry [22, 23]. The tangential and normal cutting forces on the P^{th} tooth, F_{tp} and F_{np}, are a product of the specific cutting pressures, K_t and K_n, the axial depth of cut, b, and the instantaneous chip thickness, ω_p, and are commonly expressed as

$$F_{tp} = K_t b \omega_p(t)^{\gamma} \tag{5}$$

$$F_{np} = K_t b \omega_p(t)^{\gamma} \tag{6}$$

where γ is the nonlinear relationship between the cutting force and the feed rate.

For the research performed in this paper, it was advantageous for the milling model to be converted from a rotating reference frame to a fixed reference frame, where the forces F_{tp} and F_{np} are transformed to P_x and P_y. This transformation can be expressed by

$$\begin{bmatrix} P_x \\ P_y \end{bmatrix} = \begin{bmatrix} -\cos(\theta) & -\sin(\theta) \\ \sin(\theta) & -\cos(\theta) \end{bmatrix} \begin{bmatrix} F_{xr} \\ F_{yr} \end{bmatrix} \tag{7}$$

The system dynamics of the milling operation with a compliant tool with a single mode of vibration along the *x* and *y* directions are expressed as

$$m_x \ddot{X} + c_x \dot{X} + k_x X = P_x \tag{8}$$

$$m_y \ddot{Y} + c_y \dot{Y} + k_y Y = P_y \tag{9}$$

where $\ddot{X}$, $\dot{X}$, and X are the acceleration, velocity, and displacement of the tool in the x direction, and $\ddot{Y}$, $\dot{Y}$, and Y are the acceleration, velocity, and displacement of the tool in the y direction. m_x and m_y are the modal mass in the *x* and *y* direction, $c_x$and c_y is the damping of the tool for the *x* and *y* direction, and k_x and k_y is the stiffness of the tool for the *x* and *y* direction. These equations represent the governing equations for the milling model schematic diagram shown in Figure 2.

1.4: Motivation for this Research

There are several tool displacement and chatter detection methods currently being used in research and industry. One method used in industry today is monitoring the sound waves emitted during a milling operation [19]. A disadvantage to this detection method is that chatter must occur for a short period of time before it is recognized by the monitoring system. Also, no knowledge of the tool displacement and system dynamics are acquired during this method.

Another cutting tool displacement and chatter detection system is by directly measuring the displacement of the cutting tool. Recent research at the University of Missouri [13,14] utilized such methods to analyze chatter. Capacitance sensors were placed around the tool to measure the displacement of the tool in the *x* and *y* direction. One drawback of this tool displacement measurement method is that the housing and sensors surrounding the tool restricted the reach of the cutting tool and also interfered with the automatic tool exchanger operations. Having the sensors so close to the cutting tool meant that no cutting fluid could be used, and the metal chips being flung into the air by the cutting tool could obstruct the sensors creating false readings. While these drawbacks make it impractical for industrial use, measuring the tool displacements of the cutting tool has enormous benefits pertaining to research. Measuring the tool displacements allows the system to observe the cutting tool dynamics and make changes to the milling operation long before chatter occurs. Knowledge of the cutting tool displacements can also provide accurate predictions of the surface roughness on the workpiece.

The benefits of measuring the tool displacement during milling operations make a practical tool displacement measuring system for industrial use highly desired. The research in this paper describes a new tool displacement measurement method that eliminates many of the disadvantages of the existing tool displacement measuring methods allowing it to be used in industry.

Chapter 2: Overview of Prior Cutting Tool Displacement Measurement Method

This section contains an overview of an existing cutting tool displacement and measurement method used for previous research performed at the University of Missouri. This method was employed in this research to measure tool displacement during chatter, and was also used to verify FEA results discussed in Chapter 6. An overview of the experimental setup of the existing tool displacement measurement method can be found in Section 2.1. The experimental procedure and results for the cutting tool displacement during chatter can be found in Section 2.2.

2.1: Experimental Setup of Prior Tool Displacement Measurement Method

A cutting tool displacement measurement method was previously constructed at the University of Missouri to analyze the cutting tool dynamics of a CFV1050^{si} CNC machine. For this particular CNC machine, the work table moves in the *x* and *y* direction, and the spindle moves in the z-direction. A 2-flute Robbjack EX-206-16 milling tool was used for this research. The milling tool is made of uncoated Tungsten Carbide with a 30 degree helix angle. A 6061-T6511 aluminum workpiece was bolted to the work table for experimental testing. The housing for the sensors is attached to the spindle of the CNC machine using set screws. All data collected from the sensors was collected by a data acquisition system. The experimental setup for the sensors housing mounted on the spindle and the data acquisition system can be observed in Figure 3.

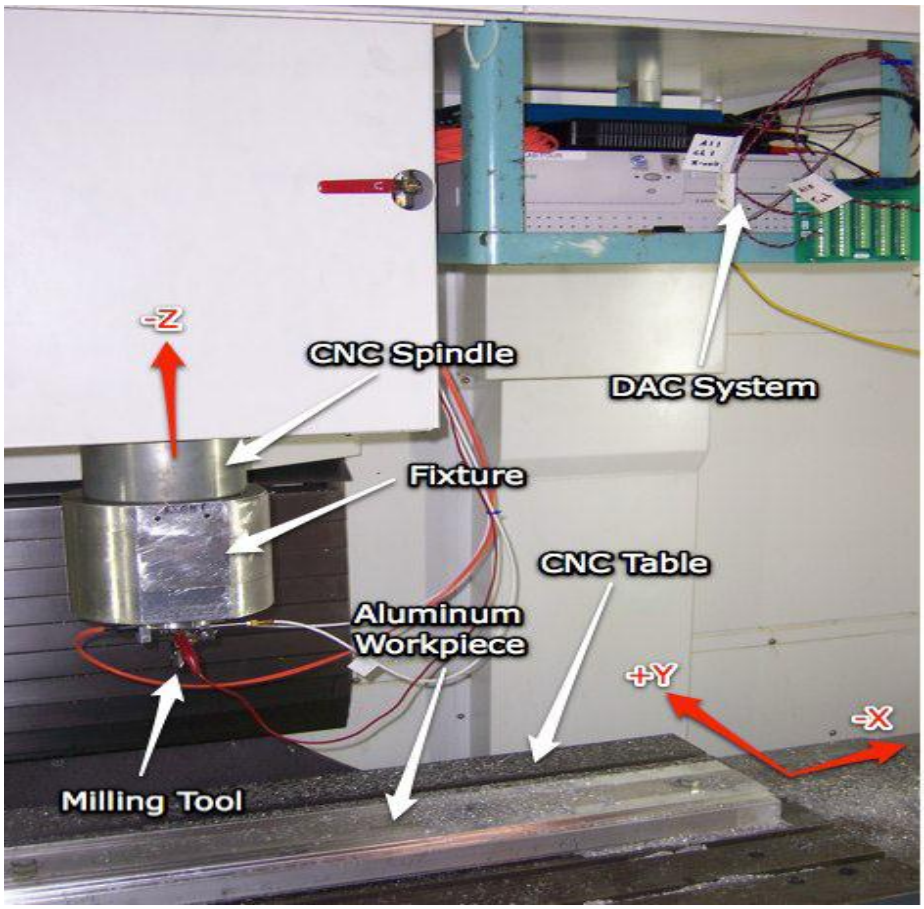

Figure 3: Experimental Setup of CNC machine with sensors housing attached to spindle. (Axis directions are shown in red).

The housing for the sensors was constructed to hold two capacitive displacement sensors perpendicular to the neck of the cutting tool to measure the tool displacement and a laser tachometer to measure the speed of the cutting tool. The capacitive sensors were placed 90 degrees apart and aligned in the appropriate orientation to measure the displacement of the cutting tool in the *x* and *y* direction. The capacitive sensors only have a sensor range of around 1 mm, so the capacitive sensors are placement at a distance of around 0.5 mm. This distance allows for a measurement of 0.5 mm in the positive and negative direction of the x and y axis. The laser tachometer was mounted on the housing 180 degrees from the x direction. For the laser tachometer to receive a signal for a completed rotation, a strip of non-reflective tape was attached to a section of the cutting tool where the laser bounced off the cutting tool. This

transition of reflective material to non-reflective material allowed the laser tachometer to produce a square wave whose frequency matched the rpm of the cutting tool. A grounding mechanism was placed in the last quadrant of the sensors housing. A bottom view of the sensors housing setup with the capacitive sensors, laser tachometer, and grounding mechanism can be observed in Figure 4.

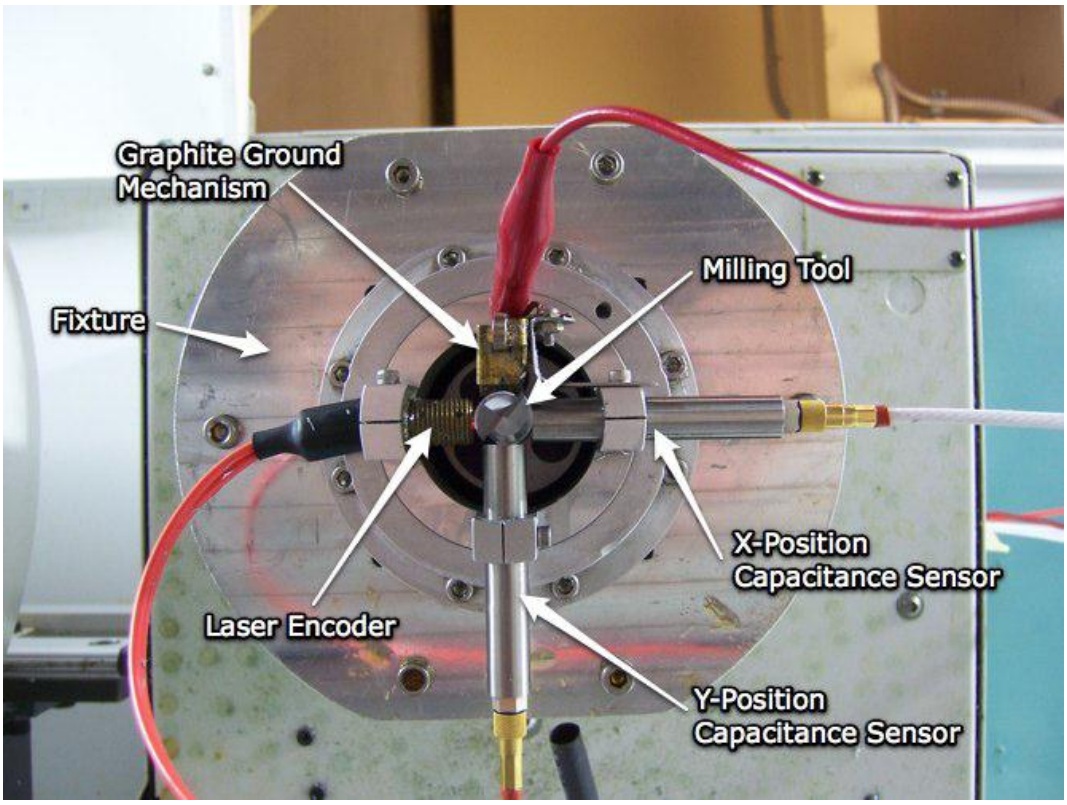

Figure 4: Bottom view of the sensors housing setup for tool displacement measurement of CNC milling operations.

2.2: Measurement of Tool Displacement during Chatter

To measure the tool displacement occurring during chatter for a typical milling operation, a milling cut was chosen that would start as a stable cut and end as an unstable cut. The point at which the cut goes from stable to unstable is known as the bifurcation point. To observe the bifurcation point, an end milling cut was performed where the depth of cut was slowly increased from 0 to 6 mm over the length of the workpiece. The bifurcation occurred at

3.55 mm depth of cut for Ω = 15000 rpm (see Figure 5). The displacement of the tool after the bifurcation point is a good representation of the chaotic movement of the cutting tool experienced during chatter.

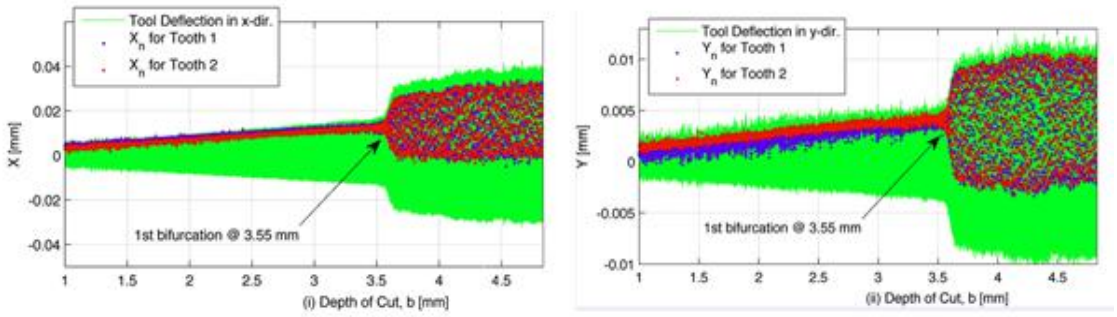

Figure 5: Experimental data for *x* and *y* displacements of cutting tool during an increasing depth of cut and Ω = 15000 rpm [13]. The red and blue dots represent the *x* and *y* displacement of the cutting tool for each tooth pass.

Chapter 3: Finite Element Analysis of Cutting Tool Experiencing Chatter

To analyze the cutting tool stress and displacement experienced during chatter, a finite element analysis was performed on the cutting tool. Creating a simulation that illustrates the displacement of the original cutting tool during chatter allows for the same simulation to be performed on the new tool design to determine if the new tool design is adequate. The cutting tool was modeled in Solidworks ® and finite element analysis was implemented using Solidworks Simulation®. The mathematical model for the approximate displacement of the cutting tool can be found in Section 3.1. The Solidworks 3D modeling of the cutting tool can be found in Section 3.2. The experimental data inputted into the Solidworks simulation can be found in Section 3.3. The chatter simulation setup and results from the Solidworks Simulation can be found in Section 3.4.

3.1: Mathematical Model for Cutting Tool Displacement

To simplify the mathematical model of the tool displacements, the neck of the cutting tool can be treated as a cylindrical cantilever beam with the fixed end being the tool holder [13]. The cutting forces P_x and P_y applied at the free end of the beam will result in the displacement of the cutting tool in the *x* and *y* direction

$$x_d(L) = \frac{P_x L^3}{3EI} \tag{10}$$

$$y_d(L) = \frac{P_y L^3}{3EI} \tag{11}$$

Where $\boldsymbol{x_d(L)}$ and $\boldsymbol{y_d(L)}$ are the displacements at the free end of the beam in the *x* and *y* direction respectively, $\boldsymbol{P_x}$ and $\boldsymbol{P_y}$ are the applied force at the free end of the beam in the *x* and *y* direction respectively, $\boldsymbol{L}$ is the length of the beam, $\boldsymbol{E}$ is the modulus of elasticity, and $\boldsymbol{I}$ is the area moment of inertia [20]. For a cylindrical beam, the area moment of inertia is

$$I = \frac{\pi r^4}{4} \tag{12}$$

Where $\boldsymbol{r}$ is the radius of the circular cross section of the cylindrical beam [21]. The angle of deflection at the free end of the cantilever beam with an applied force at the free end is given by

$$\theta_x(L) = \frac{P_x L^2}{2EI} \tag{13}$$

$$\theta_y(L) = \frac{P_y L^2}{2EI} \tag{14}$$

Where $\boldsymbol{\theta_x(L)}$ and $\boldsymbol{\theta_y(L)}$ are the angle of deflection at the free end of the beam in the *x* and *y* direction respectively.

3.2: 3D Modeling of Cutting Tool

To run a simulation on the cutting tool using the chatter tool displacement data, a solid model of the cutting tool was created using Solidworks (see fig). A digital caliper was used to find the cutting tool dimensions. The helix angle of the 2-flute Robbjack EX-206-16 milling tool was known to be 30 degrees.

A couple of slight modifications to the 3D model were made to perform the chatter simulation. A small cut was made at a height of 3.55 mm from the bottom of the cutting tool on the cutting edge for both of the cutting tool teeth. This small cut divided the cutting edge into two parts. The bottom part of the cutting edge was 3.55 mm in height and represented the cutting edge in contact with workpiece at the depth of cut of 3.55 mm. This allowed the forces in the simulation to be applied in that section of the cutting edge only.

Another slight modification was a small extrusion made 1.75 in. up from the bottom of the cutting tool. This small extrusion was used to track the displacement of the cutting tool in the *x* and *y* direction. The height of 1.75 in. up from the bottom of the tool was the position

selected for the tracker since this was the location the capacitive sensors measured the *x* and *y* displacements for the chatter tool displacement experiment described in Section 2.2.

Another modification was that the section of the cutting tool inserted into the tool holder was shortened in length. It was unnecessary to model the entire section of the unexposed tool since a small section would suffice for the applied fixtures in the simulation. Only 0.2 in of the cylindrical section of the tool portion in the tool holder was modeled. This fixed cylindrical section of the cutting tool was increased in diameter by 0.001 in so that a cylindrical face would be created in which the fixtures could be applied. Before analyzing the 3D model by the finite element method, the properties for tungsten carbide were selected for the material, and a mesh data was created from the solid model [16] (see Figure 6). Multiple mesh types were implemented on the Solidworks Simulation with negligible changes in the measurements of the tracker.

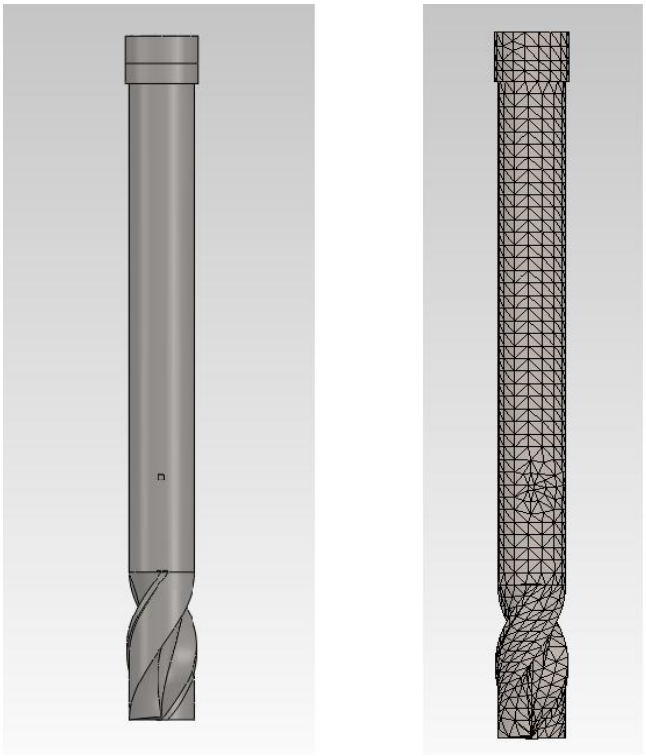

Figure 6: Solid model of cutting tool using Solidworks (left). Solid model of cutting tool with the mesh used for performing finite element method in Solidworks (right).

3.3: Experimental Data used for the Solidworks Simulation

Displacement of the cutting tool versus time data was derived from the analog signal data of the increasing depth of cut experiment described in Section 2.2 (See Figure 5). The known displacements allowed a dynamic simulation of chatter to be performed in Solidworks Simulation. To reduce the simulation run time, only 20 data points for the *x* and *y* displacements were inputted into the dynamic simulation study. While the reduced data points decrease the accuracy of the simulation, it was necessary to bring the simulation run time to a reasonable time. The data points were selected 0.1 seconds after the first bifurcation point. At a spindle speed of 15000 rpm, with data collection at 500 Hz, each data point accounted for half a revolution. The 20 data points amounted to a chatter simulation for 10 revolutions of the cutting tool.

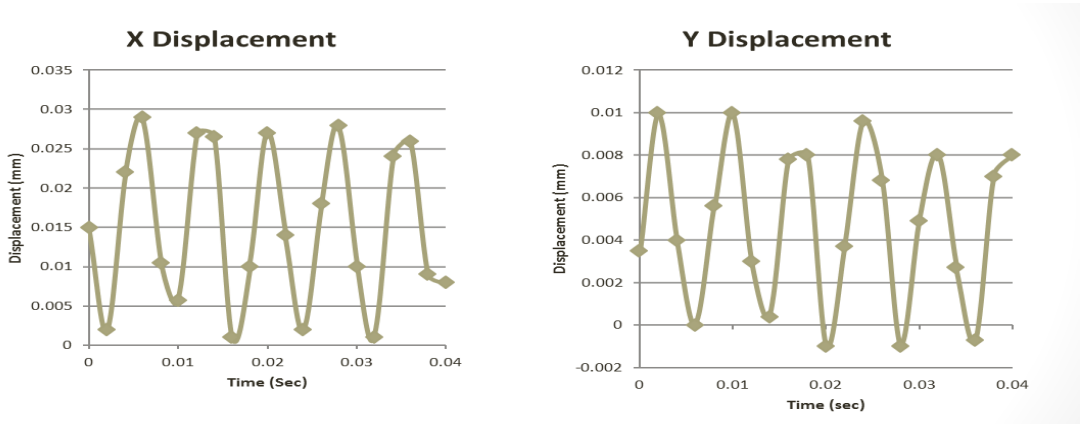

Figure 7: 20 data points from the *x* and *y* displacements 1.75 in up from the tool tip and 0.1 sec after the first bifurcation. These 20 data points were the inputted displacements for the chatter detection simulation in Solidworks. The 20 data points amounted to 10 cutting tool revolutions.

3.4: Solidworks Simulation Setup and Results for Chatter Simulation

The forces and the constraints on the cutting tool were determined before running the simulation. The constraints on the model were three types of fixtures placed on the cylindrical

face of the cutting tool portion inside the tool holder. The first type of fixture was the axial translation was set to 0, so the cutting tool was fixed in the z-direction. The second type of fixture was the radial translation was set to 0, so the cutting tool was fixed from translating in the *x* and *y* direction. The last type of fixture was the circumferential translation which was set as a linear increase from 0 to 62.83 rad over the course of the simulation. The circumferential translation allowed the tool to rotate at a constant speed for ten revolutions. This allowed the cutting tool to be oriented in the correct position for each of the 20 simulation steps.

The forces on the cutting edges were applied to the each cutting tooth's cutting edge in contact with the workpiece as described in Section 3.2. The *x* and *y* cutting forces applied on the cutting edge were oriented in the *x* and *y* direction and did not change direction as the tool rotated (see Figure 8).

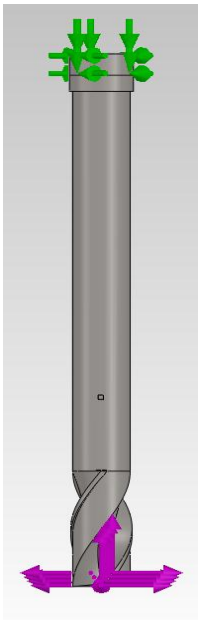

Figure 8: Solidworks Simulation setup for the cutting tool chatter FEA. The small cylinder at the top is the part of the tool fixed by the tool holder. The green arrows represent the fixtures applied on the cylindrical face. The purple arrows on the cutting tool edge represent the cutting force in the *x* and *y* direction.

20 static studies were performed on the tool to achieve the displacements from the experimental data. The tracker was utilized on all 20 static studies to check the *x* and *y*

displacements for each of the 20 data points. The forces in the *x* and *y* direction were changed for each static study until the desired tool displacement (Figure 7) in the *x* and *y* direction was achieved. The forces used to achieve each of the *x* and *y* displacements in each of the 20 static studies were recorded.

A dynamic study was performed on the cutting tool using the 20 *x* and *y* forces from the static studies as the inputted forces. The forces were applied at the same time interval as the experimental data so the FEA dynamic study became a simulation of the chatter in the cutting tool experienced 0.1 seconds after the bifurcation point. A scaled version of the displacement over time for the dynamic study makes the deformation of the cutting tool more obvious. Observing the deformation of the cutting tool makes the curvature formed in the neck of the cutting tool clear (see Figure 9).

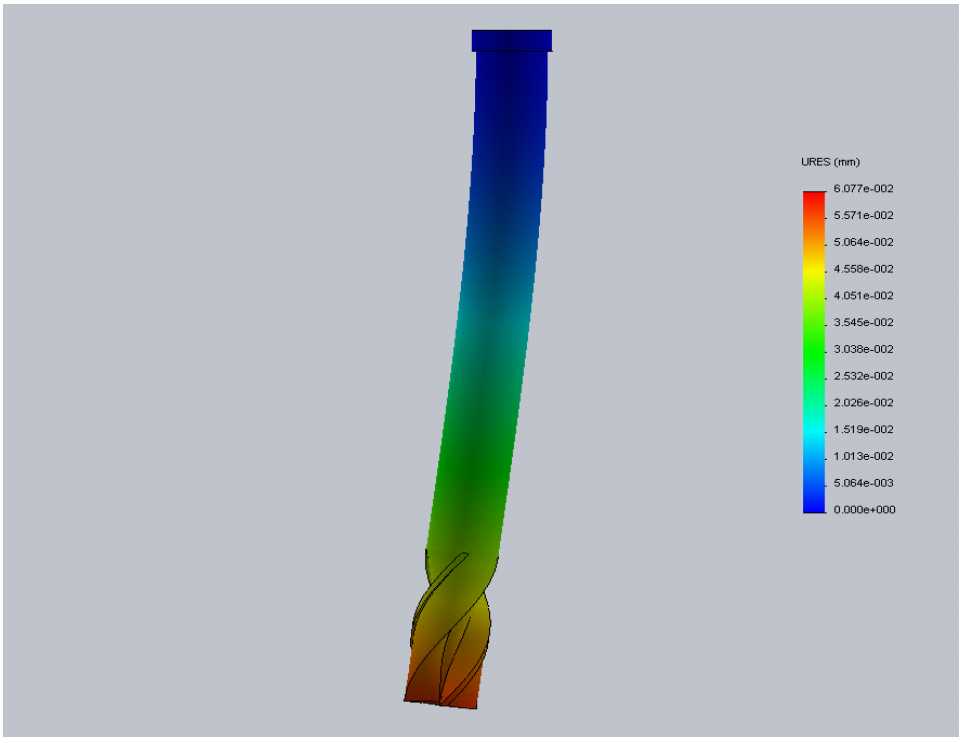

Figure 9: Screen shot from the side view of cutting tool FEA while tool is undergoing chatter simulation. The colors represent the magnitude of displacement in the tool according to the color legend.

Chapter 4: New Tool Design

In this Chapter the new tool design is presented. A mathematical model and FEA analysis are performed on the new tool design to determine the necessary radius and height of the thin disc on the cutting tool neck. The conceptual basis and benefits of the new tool design can be found in Section 4.1. The mathematical model for the new cutting tool can be found in Section 4.2. A finite element analysis on the new tool design can be found in Section 4.3. The fabrication of the experimental cutting tool with disc can be found in Section 4.4.

4.1: Conceptual Basis and Benefits of New Tool Design

The curvature in the neck of the tool that occurs during tool displacement is the basis behind the research presented in this paper. A new tool design was created to capture this curvature in the neck of the cutting tool and create a new technique for tool displacement measurement. The concept of the new tool is to modify the tool design with the addition of a thin circular disc connected perpendicular to the neck of the cutting tool (See Figure 10)

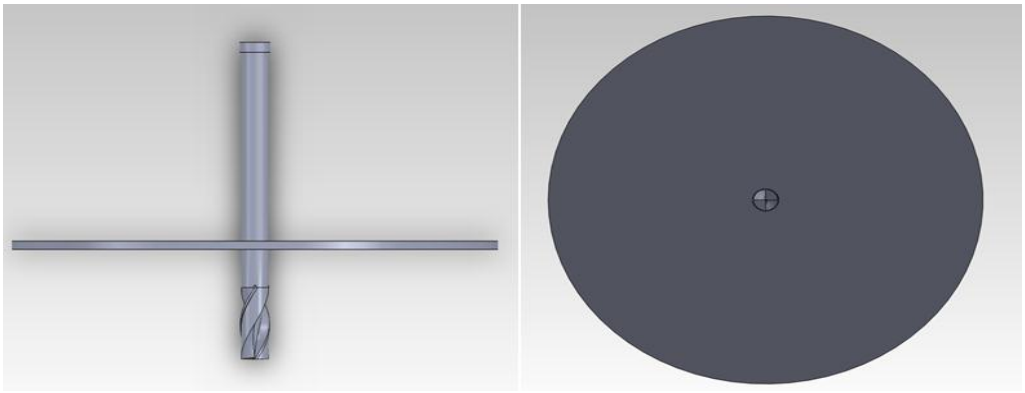

Figure 10: New cutting tool design with the thin disc addition attached at 1.75 in. from the bottom of the cutting tool.

When the new cutting tool is experiencing tool displacement, the neck of the cutting tool will become curved. The curvature in the new cutting tool neck will cause the attached disc

to tilt. The tilting of the disc will cause a displacement of the disc in the z-direction allowing sensors to measure the tool displacement from above.

There are numerous benefits to this tool displacement measurement method over the previous method used at the University of Missouri. The main benefit of this new tool displacement measurement method is that the displacement sensors can be placed up above the cutting tool and out of the way, getting rid of the need for a large sensors housing. Having the sensors located away from the cutting tool means no interference between the workpiece and the sensors will occur. Also, having the sensors away from the cutting tool allows for the use of cutting fluid in milling operations which would have ruined the sensors in the previous displacement measurement setup. Eliminating the large sensors housing also allows for the automatic tool exchanger to become functional while the displacement sensor is also used.

The disc itself is a benefit to the tool displacement measurement method since it will shield the sensors from any chips or cutting fluid being flung into the air by the cutting tool.

The main goal of measuring the tool displacement using this method would be to eliminate the onset of chatter in high speed milling. With sensors monitoring the tool displacement, it would be possible for the CNC machine to recognize the increase in tool displacement before chatter occurs (see Figure 5). Recognizing the tool is on the verge of chatter will allow the CNC machine to make alterations to the milling procedure before chatter begins, essentially eliminating chatter.

4.2: Mathematical Model of New Tool Design

Determining the size and location of the thin disc on the neck of the cutting tool is a critical part in designing the new tool. The disc isn't located at the free end of the beam, so the displacement of a cantilever beam at a given point along the beam with a load at the free end is given as

$$x_d(a) = \frac{P_x}{6EI}(2L^3 - 3L^2a + a^3) \quad \text{and} \tag{15}$$

$$y_d(a) = \frac{P_y}{6EI}(2L^3 - 3L^2a + a^3) \tag{16}$$

Where $\boldsymbol{x_d(a)}$ and $\boldsymbol{y_d(a)}$ are the displacements of the beam in the *x* and *y* direction at distance $\boldsymbol{a}$ from the free end, $\boldsymbol{P_x}$ and $\boldsymbol{P_y}$ are the applied force in the *x* and *y* direction at the free end of the beam, $\boldsymbol{L}$ is the length of the beam, $\boldsymbol{E}$ is the modulus of elasticity, $\boldsymbol{I}$ is the area moment of inertia [20]. The angle of deflection at a given distance from the free end of the beam with a load at the free end is given as

$$\theta_x(a) = \frac{P_x}{2EI}(L^2 - a^2) \quad \text{and} \tag{17}$$

$$\theta_y(a) = \frac{P_y}{2EI}(L^2 - a^2) \tag{18}$$

The symbol $\boldsymbol{\theta_x(a)}$ is the angle of rotation about the y axis due to a force in the x direction at distance $\boldsymbol{a}$ from the free end and $\boldsymbol{\theta_y(a)}$ is the angle of rotation about the x axis due to a force in the y direction at distance $\boldsymbol{a}$ from the free end. $\boldsymbol{P_x}$ and $\boldsymbol{P_y}$ are the applied force in the *x* and *y* direction at the free end of the beam, $\boldsymbol{L}$ is the length of the beam, $\boldsymbol{E}$ is the modulus of elasticity, $\boldsymbol{I}$ is the area moment of inertia [20].

The sensors above the disc would be located near the edge of the disc to pick up the maximum displacement of the disc in the z-direction. The displacement of the edge of the disc in the z-direction will be

$$Z_d = r_d \sin(\theta) \tag{19}$$

where $\boldsymbol{Z_d}$ is the displacement of the disc in the z direction, $\boldsymbol{r_d}$ is the radius of the disc, and $\boldsymbol{\theta}$ is the angle of deflection of the cutting tool.

Using Equations 15-19, a direct relation between the displacement of the disc in the z direction and the displacement of the cutting tool in the *x* and *y* direction is given as

$$x_d(z_{dx}) = \frac{\sin^{-1}\left(\frac{z_{dx}}{r}\right)(2L^3 - 3L^2a + a^3)}{3(L^2 - a^2)} \quad \text{and} \quad (20)$$

$$y_d(z_{dy}) = \frac{\sin^{-1}\left(\frac{z_{dy}}{r}\right)(2L^3 - 3L^2a + a^3)}{3(L^2 - a^2)} \quad (21)$$

where the disc is located at a distance $\boldsymbol{a}$ from the cutting tool tip, $\boldsymbol{x_d(z_{dx})}$ and $\boldsymbol{y_d(z_{dy})}$ are the displacements of the tool at the height of the disc in the *x* and *y* direction respectively, ***r*** is the radius of the disc at which the sensors are located, ***L*** is the length of the cutting tool from tip to tool holder, and $\boldsymbol{z_{dx}}$ and $\boldsymbol{z_{dy}}$ are the displacements of the disc in the z direction measured above the *x* and *y* axis respectively.

4.3: Finite Element Analysis of New Tool Design

A finite element analysis was performed on the new tool design in order to figure out the necessary location and radius of the disc to achieve substantial displacements in the z-direction. A large thin disc with a diameter of 8 in was modeled in Solidworks and was attached perpendicular to the neck of the cutting tool (see fig.). A fine mesh was created for the new tool design (see Figure 11).

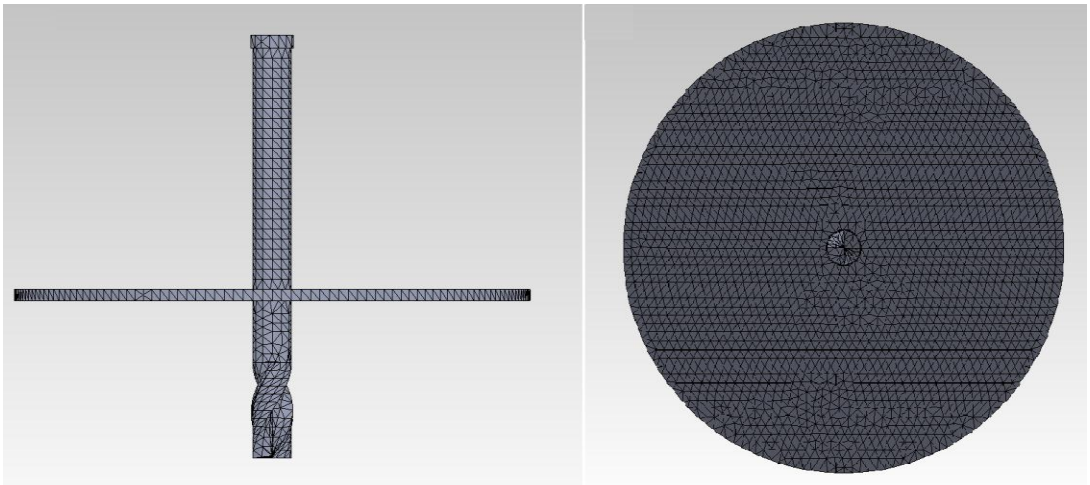

Figure 11: FEA mesh construction for the cutting tool with thin disc attached at 1.75 in. from the bottom of the cutting tool.

The cutting tool with the disc was put through the same chatter simulation dynamic study that was performed on the cutting tool as described in Section 3.4. The large disc allowed for a wide range of disc radii to be observed from one analysis. The tilt of the disc experienced during the chatter simulation becomes obvious when a scaled deformation is shown (see Figure 12).

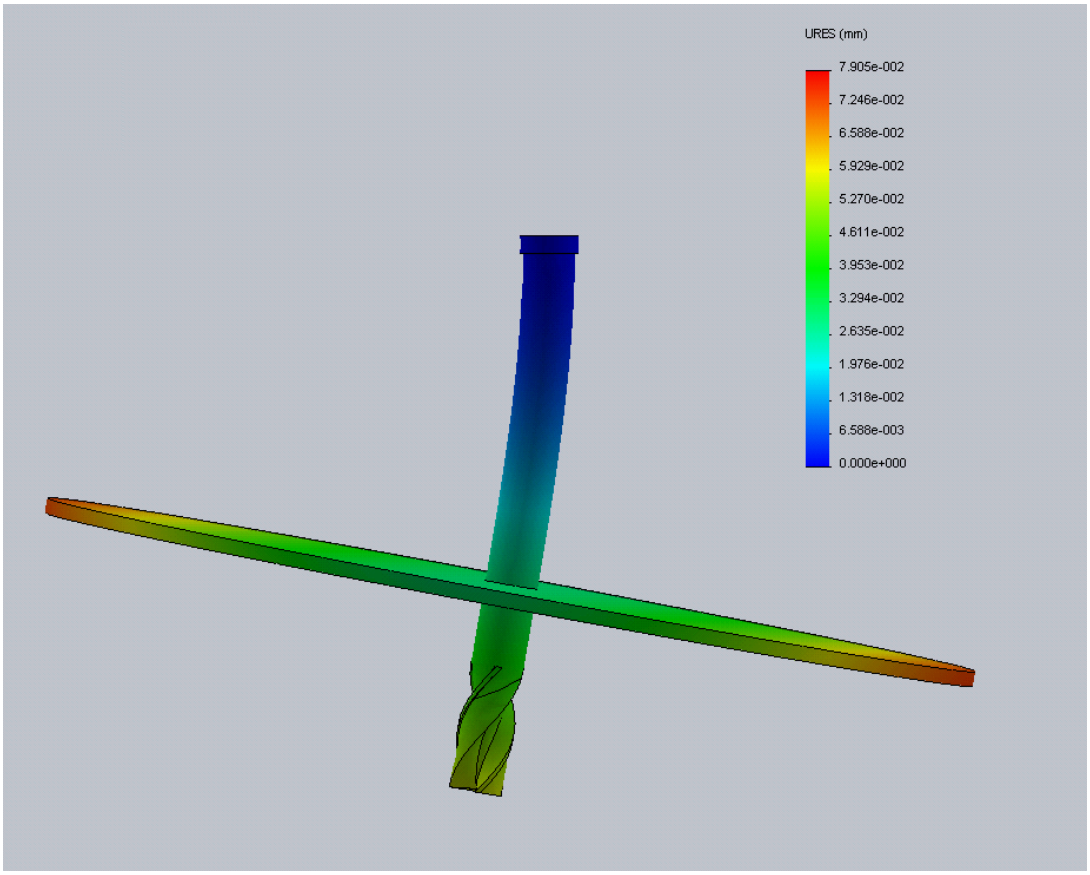

Figure 12: Side view screen shot of the cutting tool with disc attached 1.75 in. from the bottom of the cutting tool FEA while tool is undergoing chatter simulation. The colors represent the magnitude of displacement in the tool according to the color legend.

From Figure 12, it is clear that the large disc undergoes substantial tilt 1.75 in from the cutting tool tip. The displacement of the disc in the z direction is more than sufficient to be within the range of a displacement sensor.

A second finite element analysis was performed with the disc located 4.25 in from the cutting tool tip. From Equations 17 and 18, it's clear that the height of the disc on the cutting

tool neck affects the angle of tilt of the disc. The chatter simulation dynamic study was performed on the cutting tool with the disc at the new height. The maximum tilt was much smaller for the higher disc, but the displacement near the edge of the disc was still well within the range of a displacement sensor (see Figure 13).

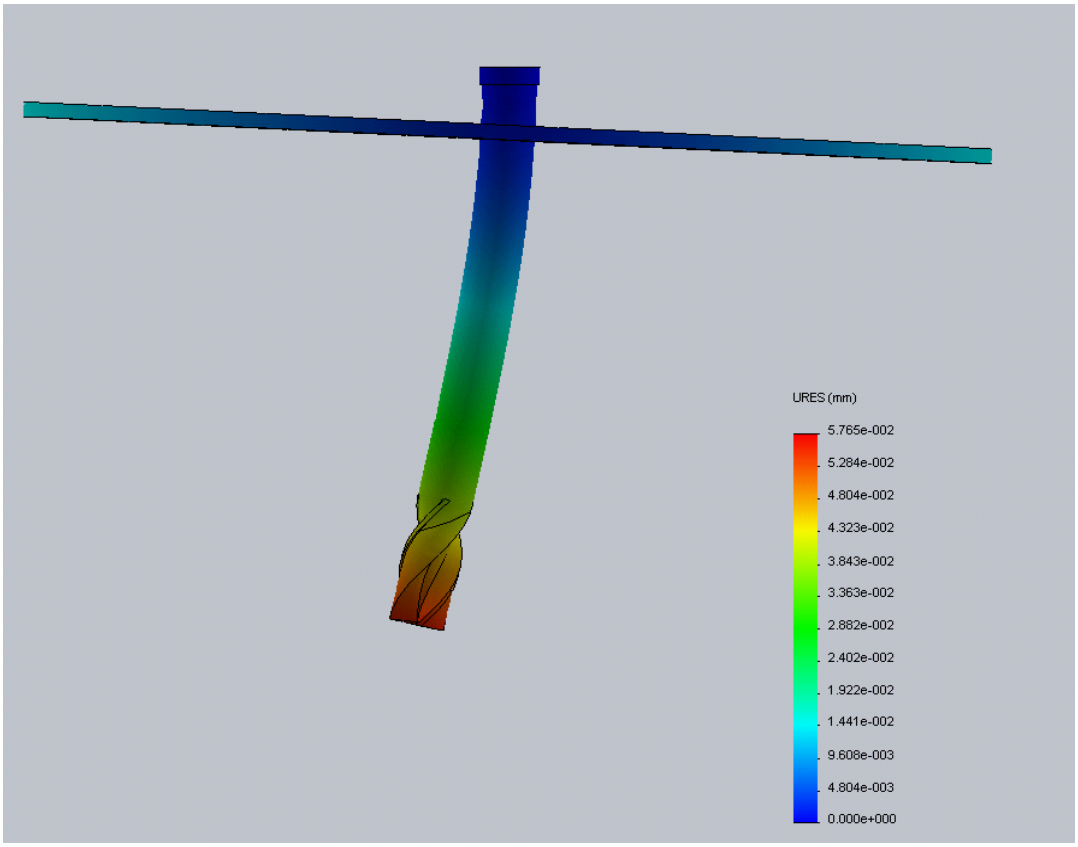

Figure 13: Side view screen shot of the cutting tool with disc attached 4.25 in. from the bottom of the cutting tool FEA while tool is undergoing chatter simulation. The colors represent the magnitude of displacement in the tool according to the color legend.

4.4: Fabrication of Experimental New Cutting Tool Design

The manufacturing of a new tool with a thin disc attached would be too expensive for this research. Instead, a thin disc was manufactured to be attached to the existing 2-flute Robbjack EX-206-16 milling tool (See Figure 14). The cutting tool had a diameter of 0.5 in, so the disc had an inner diameter of 0.501 in to allow the tool to pass through. The outer diameter of the disc was 8 in. The thickness of the disc was 0.04 in which was thin enough to make the disc

lightweight, but thick enough to make the disc rigid. A rigid disc was desired for this experiment so that the displacement of the disc directly reflected the tilt of the disc resulting from the curvature in the neck of the tool.

To attach the disc to the cutting tool, two balanced clamp-type collars are used to sandwich the disc at a desired location along the tool neck. The balanced clamp-type collar collars are tightened by two opposing screws. The opposing screw directions oriented the screws to act as counter weights to prevent any induced vibrations from unbalanced weight distribution when the tool was rotating. In addition to the balanced clamp collars, a square piece of tape is placed on each side of the disc between the clamp collars and the disc. The mounting tape prevents the disc from slipping and spinning between the pair of clamp collars. Since the tape is square and symmetrical, the weight is balanced to prevent any induced vibrations when the tool is rotating.

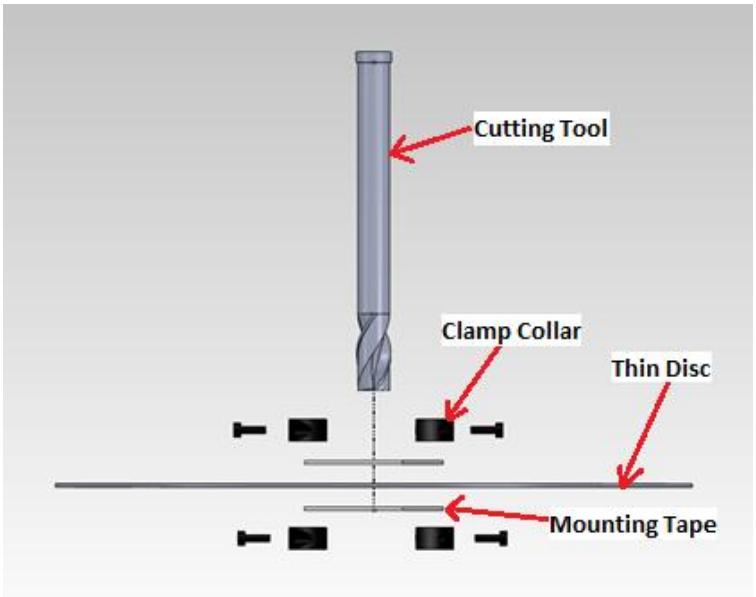

Figure 14: Exploded front view of tool with disc setup. Double sided tape is placed in between the clamp collars and the disc to prevent the disc from rotating. The clamp collars are tightened and used to sandwich the disc at a desired height on the neck of the tool.

Once the disc is attached to the cutting tool, the clamp collars can be loosed to slide the disc up or down the neck of cutting tool to a new desired location and then retightened. This

allows for easy testing of the disc at different heights on the neck of cutting tool. A level was used for every height change to ensure that the disc remained flat. The completed assembly for the experimental new tool with disc can be seen in Figure 15.

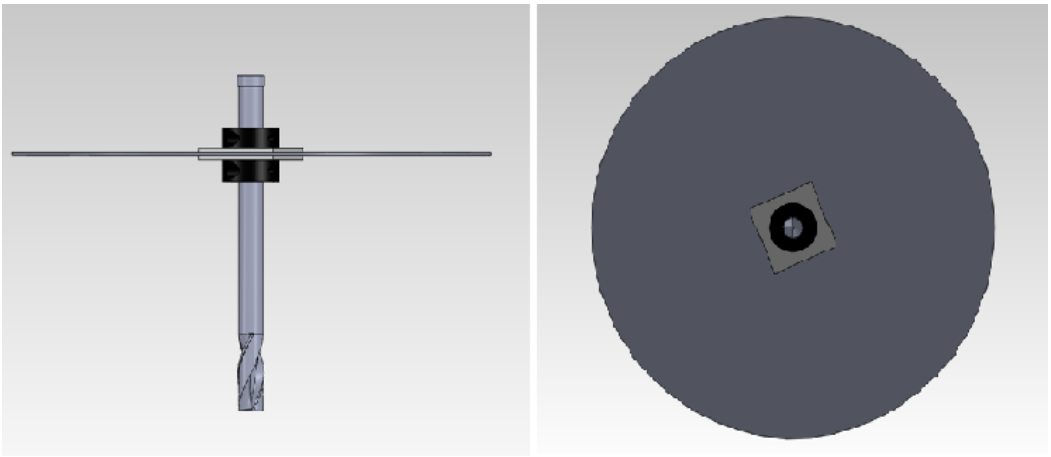

Figure 15: Front view of the experimental tool with disc (left). Bottom view of the experimental tool with disc (right).

Chapter 5: Determining the Cutting Forces of Cutting Tool with and without the Thin Disc Attached.

In this section, the cutting forces for a slot milling cut are found for the cutting tool with and without the disc using a rotating cutting force dynamometer. A difference in the cutting force between the two tools would mean that the stable region for milling would be different. If the cutting force becomes too large with the addition of the disc, then the cutting teeth may become more susceptible to wear and breakage. The installation of the dynamometer can be found in Section 5.1. The calibration of the dynamometer can be found in Section 5.2. The experimental procedure and results for the cutting forces measurement of the cutting tool with and without the thin disc can be found in Section 5.3. The comparison of the cutting forces of the tool with and without the thin disc can be found in Section 5.4.

5.1: Installation of Dynamometer and Stator

To obtain the cutting forces, a rotating cutting force dynamometer was utilized in the experiments. The rotating cutting force dynamometer is used for the dynamic and quasistatic measurement of the three force components P_x, P_y, P_z as well as the drive moment M_z on a rotating tool [15].

To install the dynamometer, the tool unclamp command was initiated while the dynamometer was fitted into the CNC machine spindle. Once the dynamometer was in place, the tool unclamp command was released and the dynamometer was locked in the spindle.

To receive the data collected by the dynamometer, the stator must be mounted concentric with the dynamometer while maintaining a gap of 1 to 2 mm [15]. To install the stator at this location, two identical mounting bracket halves were manufactured to securely hang the stator (See Figure 16).

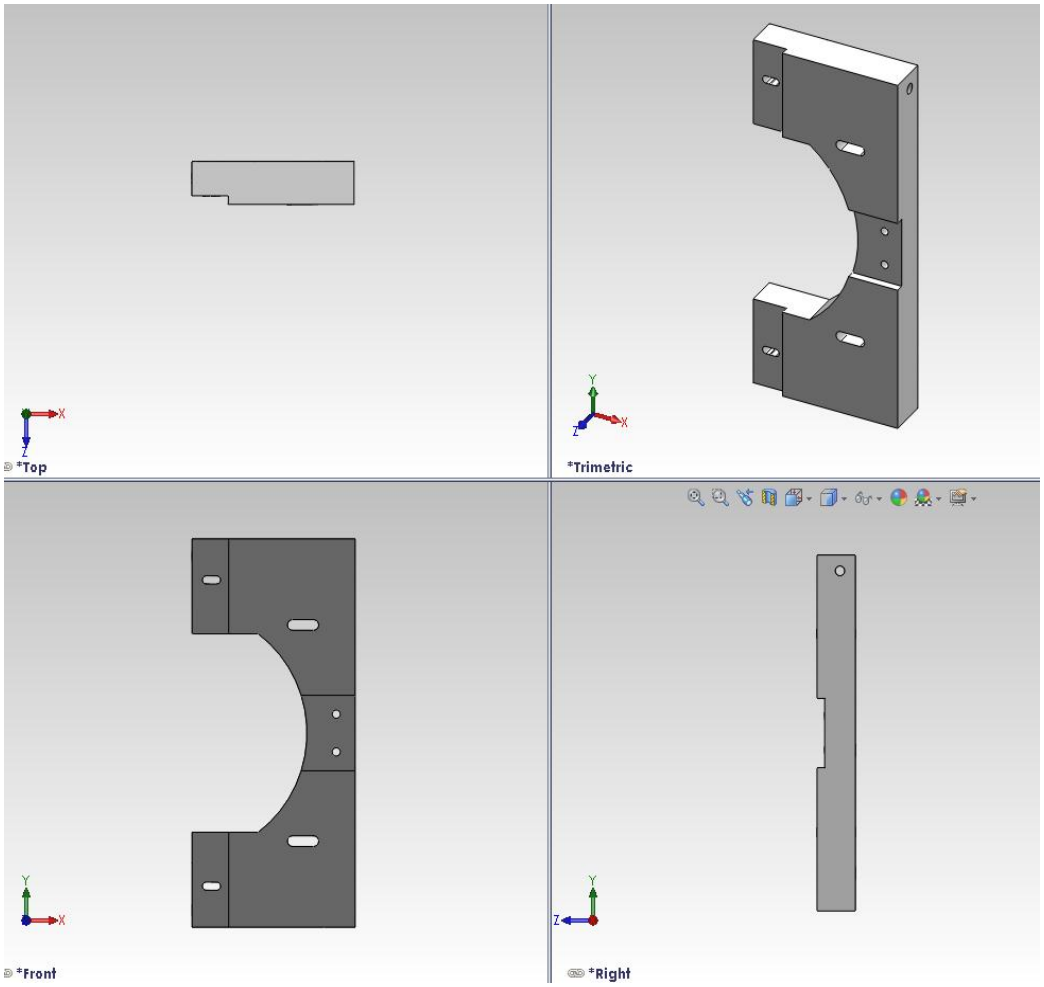

Figure 16: Top, front, side, and trimetric view of a mounting bracket half. Part was designed in Solidworks and machined in the machine lab.

Each mounting bracket half fitted snugly onto one half of the stationary part of the spindle. Two long screws connected the two mounting bracket halves together. A small gap between the two mounting bracket halves allowed the screws to tighten until the two mounting bracket halves tightly clamped onto the spindle (See Figure 17).

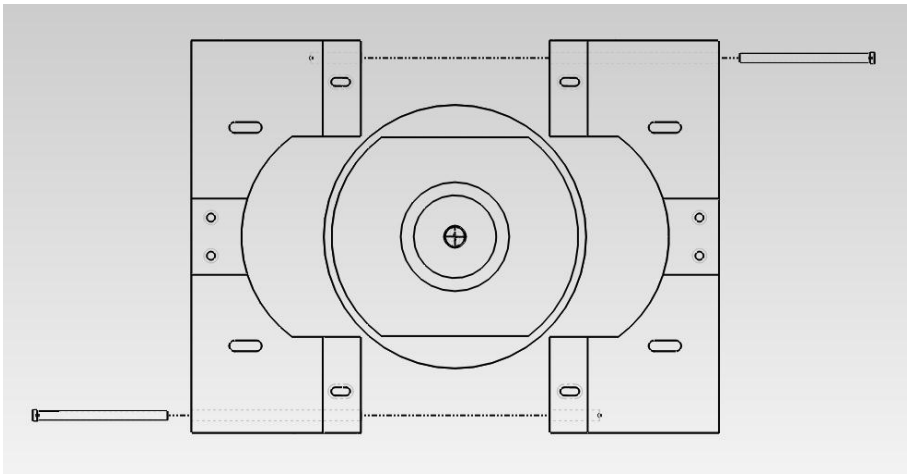

Figure 17: Exploded bottom view of bracket setup (hidden lines visible). One long screw is inserted into one side of each bracket half and screwed into the internal threading of the opposing bracket half. The screws are tightened until the bracket is tightly secured onto the spindle.

One of the mounting bracket halves would hold the stator. Slots in the mounting bracket allowed for the stator's positioning to adjust in order to achieve the desired 1 to 2 mm gap between the stator and the dynamometer. The stator was connected to the mounting bracket half by a pair of long screws and nuts. Two spacers were also included in the assembly to place the stator at the correct height and make the assembly rigid (See Figure 18). The final step in the installation of the dynamometer is to place to the cutting tool in the tool holder at the bottom of the dynamometer and lock it in place using a set screw (See Figure 19).

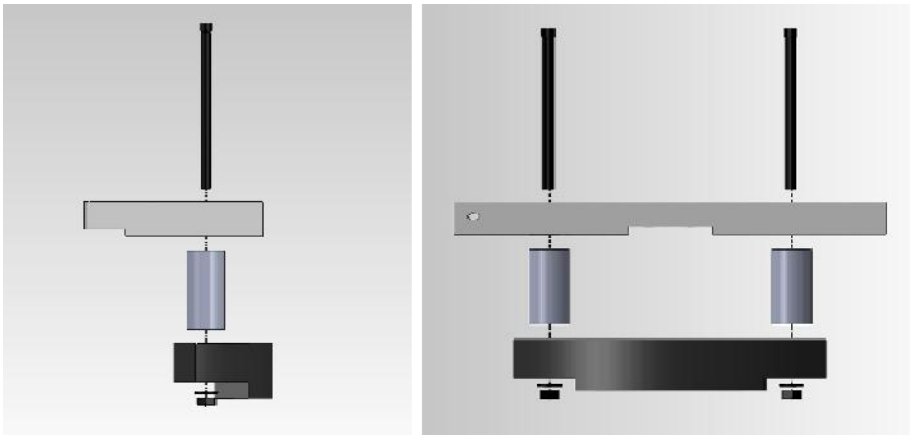

Figure 18: Exploded front view of stator attached to the mounting bracket half (left). Exploded side view of the stator attached to the mounting bracket half (right).

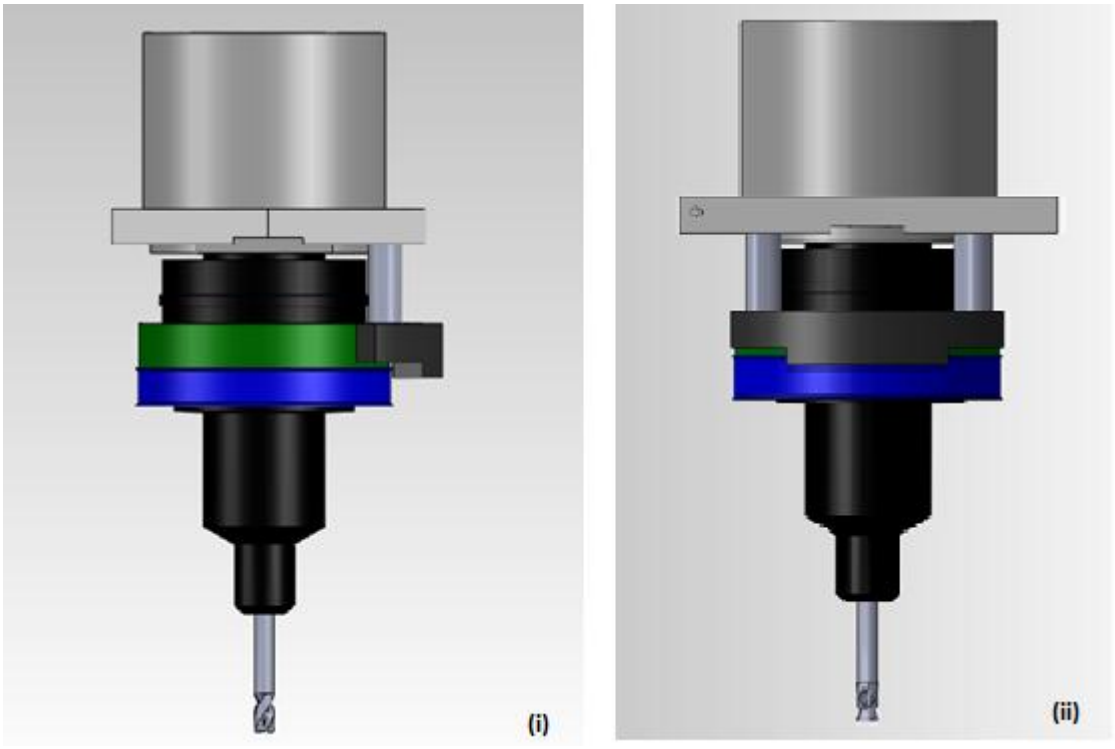

Figure 19: Front view of dynamometer with stator setup (i). Side view of dynamometer with stator setup (ii). The stator is concentric with the dynamometer and spaced a few millimeters away from the dynamometer to allow the dynamometer to rotate, but still close enough to pick up the signal.

5.2: Calibrating the Dynamometer

The acquired data from the dynamometer included the force in the x, y, and z directions and the torque in the clock-wise and counter clock-wise directions. To determine all of the calibration constants for the dynamometer, five calibration procedures were performed.

Labview® was the chosen computer program for the data acquisition and displayed the data in the form of analog signals. The signals from the stator were first processed in the multichannel signal conditioner (See Figure 20). The multichannel signal conditioner was set to the fine range since the measured forces were well within the fine range for all of the sensors. Five connecting cables were used to transmit the data from the multichannel signal conditioner to the signal condition hooked up to the PC with Labview. One connecting cable was needed for

each of the five channels. The five channels were the force in the x direction, the force in the y direction, the force in the z direction, the torque, and the zero count signal. The minimum sampling frequency for sampling the zero count signal is 4000 Hz [15]. Lower sampling rates may miss some of the zero count signals resulting in a lower measured spindle speed. To ensure the correct measured spindle speed and to achieve clear data results, a sampling rate of 40 kHz was chosen for all of the dynamometer experiments.

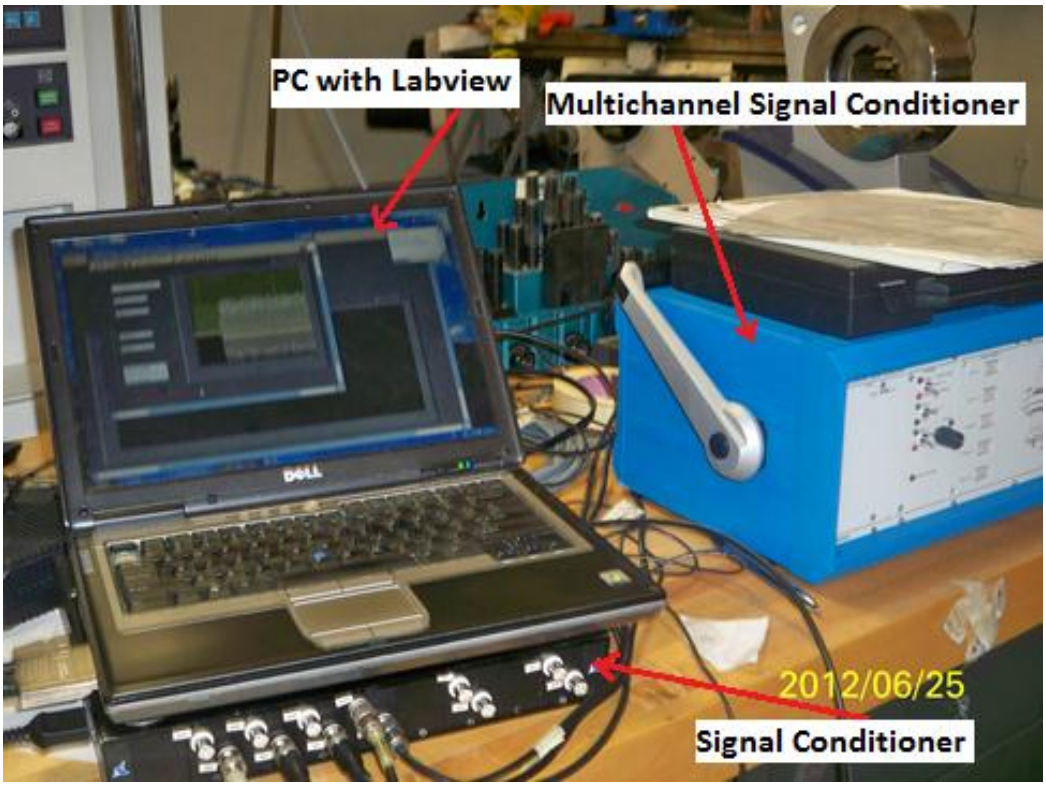

Figure 20: Data collecting setup for the dynamometer experiments. Signal went from the stator to the multichannel signal conditioner and then to the signal conditioner connected to the PC. The data was then collected and saved onto The PC using Labview.

The full calibration of the dynamometer procedure can be found in appendix A. The results from the calibration tests were compared to the manufacturer's calibration certificate (see Table 1). All of the experimental results of the calibration constants were near the manufacturer's given calibration constants with an average percent error of 4.66%.

Table 1: Comparison of the experimental calibration constants versus the manufacturer's calibration constants for the fine range of the multichannel signal conditioner. Average percent error was 4.66%.

Sensor Direction	Experimental Calibration Constant (Fine Range)	Manufacturer's Calibration Constant (Fine Range)	% Error
X-Direction	5.53 mV/N	5.31 mV/N	4.143%
Y-Direction	5.66 mV/N	5.40 mV/N	4.815%
Z-Direction	3.00 mV/N	3.35 mV/N	10.45%
Torque (CW)	87.1 mV/Nm	87.9 mV/Nm	0.9101%
Torque (CCW)	-88.6 mV/Nm	-85.5 mV/Nm	3.626%

5.3: Experimental Procedure and Results for Measuring the Cutting Forces

The cutting forces were found for the uncoated 2-flute Robbjack EX-206-16 milling tool with and without the disc. The material of the workpiece was Aluminum 6061-T6511. To secure the workpiece to the CNC worktable, a large vise was fastened onto the worktable. The screw holes in the CNC worktable and the vise ensured that the vise was aligned with the *x* and *y* directions.

The Aluminum 6061 T-6511 workpiece was placed flat into the vice and the vice was clamped tight to secure the workpiece. The surface of the Aluminum 6061-T6511 workpiece was face milled flat using a larger cutting tool to quickly obtain a clean surface and assure that top of the workpiece was parallel with the *xy* plane.

5.3.1: Measuring the Cutting Forces for the Cutting Tool without the Disc Attached

The 2-flute Robbjack EX-206-16 milling tool was placed in the dynamometer tool holder and locked in place using the dynamometer set screw. The CNC machine absolute coordinate system is zeroed at the upper top left corner of the workpiece to establish a coordinate system

on the workpiece with the origin at the corner. This was achieved by zeroing the x, y, and z axis one at a time. The CNC hand wheel was used to slowly move the cutting tool towards the workpiece edge until contact is made and the coordinate was zeroed for that direction. Once the coordinate system was established, the experimental setup was complete and data collection commenced (see Figure 21).

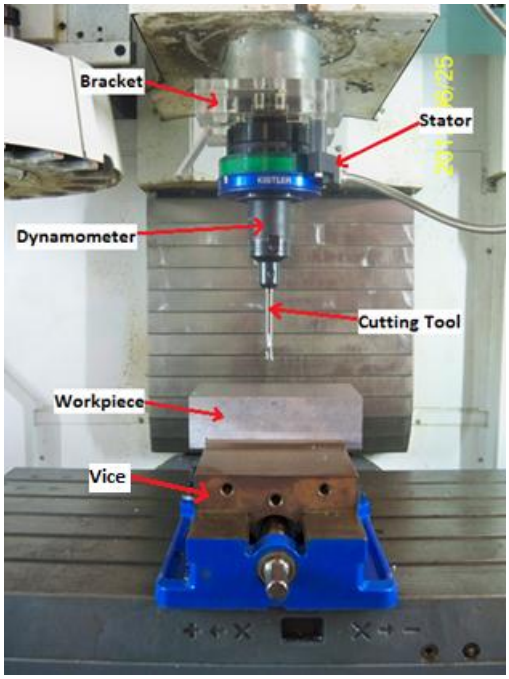

Figure 21: Experimental setup for the dynamometer to determine the cutting forces of the uncoated 30 degree helix angle cutting tool without the disc.

To obtain the cutting forces data, slot milling cuts were performed at a depth of 2 mm and a spindle speed of 200 rpm. The slot was milled until the cutting tool was fully immersed into the workpiece before data was collected. The starting feed rate for data collection was 0.05 mm/rev, and was increased in increments of 0.05 mm/rev to a final feed rate of 0.3 mm/rev. This allowed for a range of cutting forces to be found for the cutting tool. The voltage signal from the Labview program was multiplied by the calibration coefficients in Table 1 to output the measured force. Since the dynamometer is rotating while measuring the *x* and *y* cutting forces, the measured *x* and *y* forces were actually the tangential and radial cutting forces. The measured forces *x* and *y* forces were transformed from the rotating coordinate system to the

fixed coordinate system using Equation 7. The cutting forces in the *x* and *y* direction of the fixed coordinate system for each feed rate can be observed in Figures 22-27.

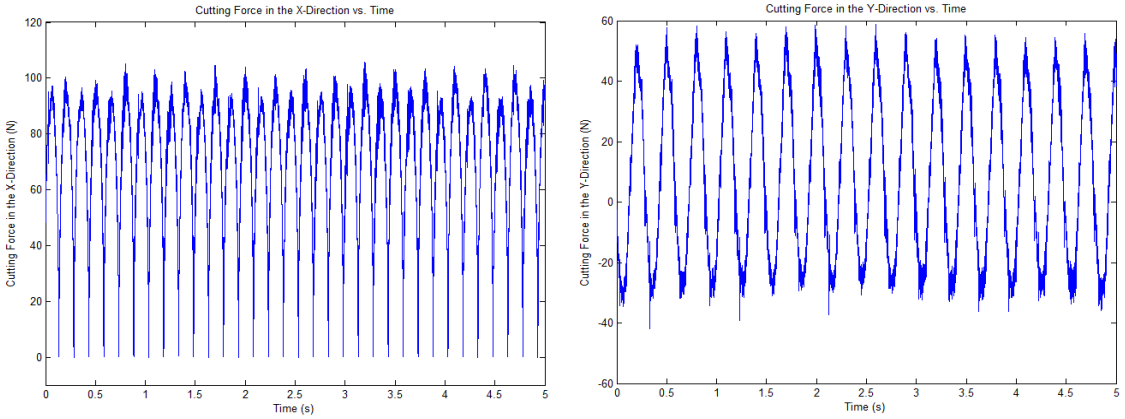

Figure 22: Slot milling cut was made at 2 mm depth of cut, spindle speed of 200 rpm, and a feed rate of 0.05 mm/rev. Cutting Forces in the *x* and *y* direction for the cutting tool without the disc.

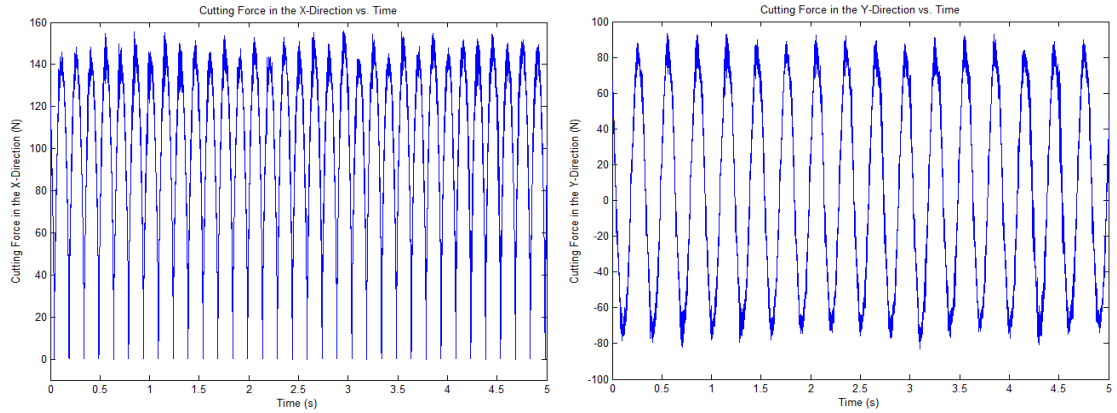

Figure 23: Slot milling cut was made at 2 mm depth of cut, spindle speed of 200 rpm, and a feed rate of 0.10 mm/rev. Cutting Forces in the x and y direction for the cutting tool without the disc.

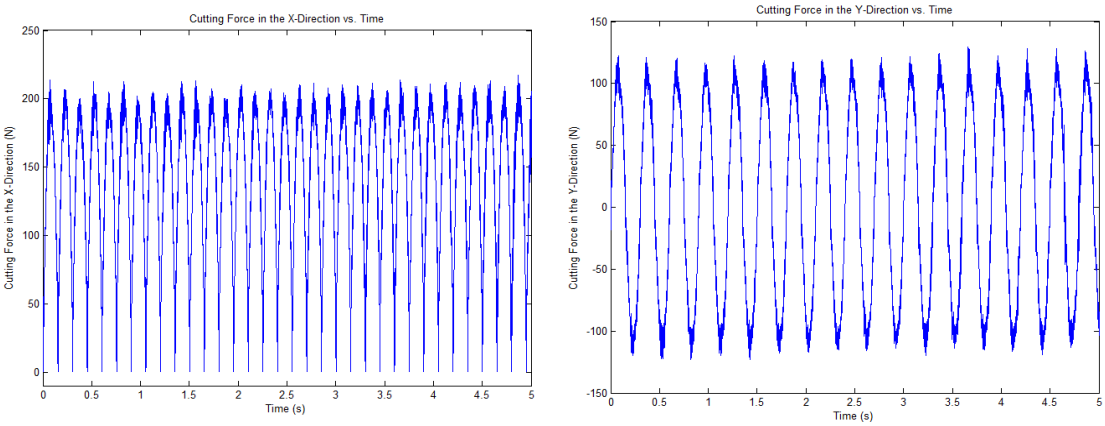

Figure 24: Slot milling cut was made at 2 mm depth of cut, spindle speed of 200 rpm, and a feed rate of 0.15 mm/rev. Cutting Forces in the x and y direction for the cutting tool without the disc.

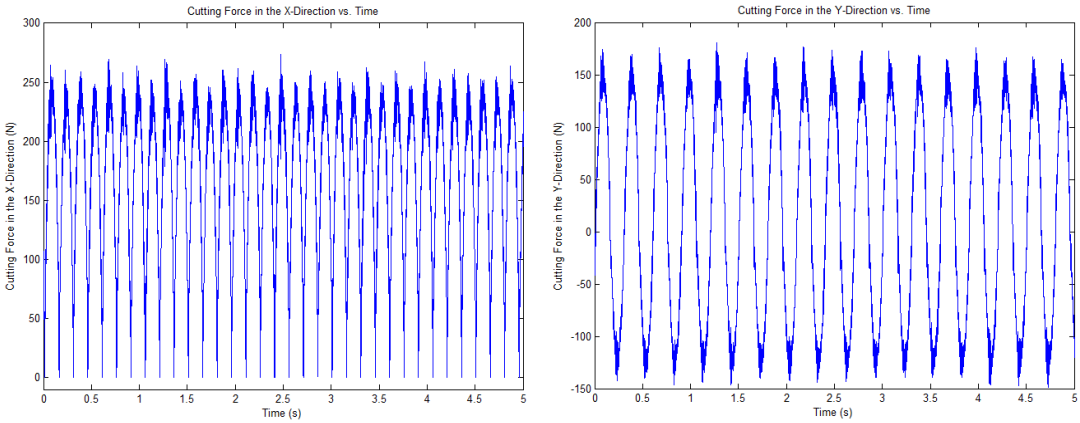

Figure 25: Slot milling cut was made at 2 mm depth of cut, spindle speed of 200 rpm, and a feed rate of 0.20 mm/rev. Cutting Forces in the x and y direction for the cutting tool without the disc.

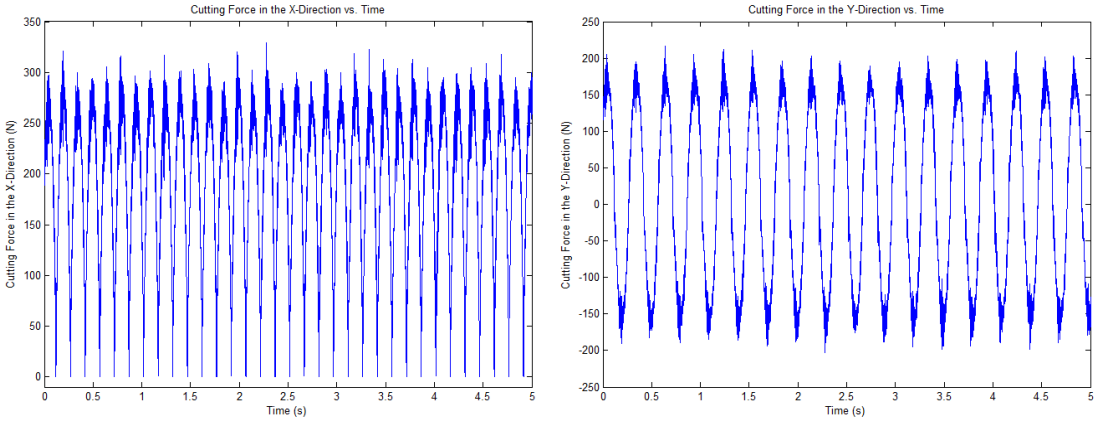

Figure 26: Slot milling cut was made at 2 mm depth of cut, spindle speed of 200 rpm, and a feed rate of 0.25 mm/rev. Cutting Forces in the x and y direction for the cutting tool without the disc.

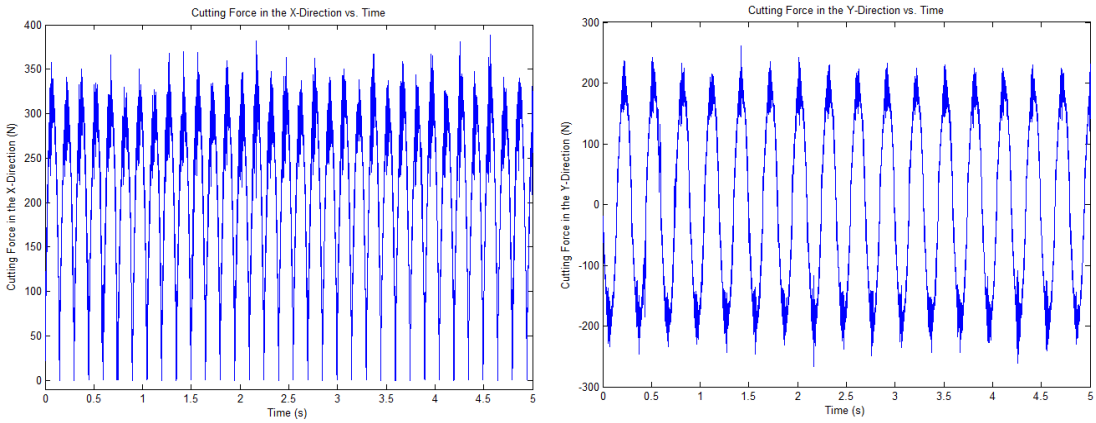

Figure 27: Slot milling cut was made at 2 mm depth of cut, spindle speed of 200 rpm, and a feed rate of 0.30 mm/rev. Cutting Forces in the x and y direction for the cutting tool without the disc.

5.3.2: Measuring the Cutting Forces for the Cutting Tool with the Disc Attached

The thin disc was attached to the 2-flute Robbjack EX-206-16 milling tool by using the method described in Section 4.4 (see Figure 28). The same slot milling cuts as described in Section 5.3.1 were performed for the cutting tool with the disc so comparisons of the cutting forces for the tool with and without the disc can be established. The same process as described in Section 5.3.1 was employed to transform the measured voltage signal into the cutting forces in the fixed *x* and *y* direction. The cutting forces in the *x* and *y* direction of the fixed coordinate system for each feed rate can be observed in Figures 29-34.

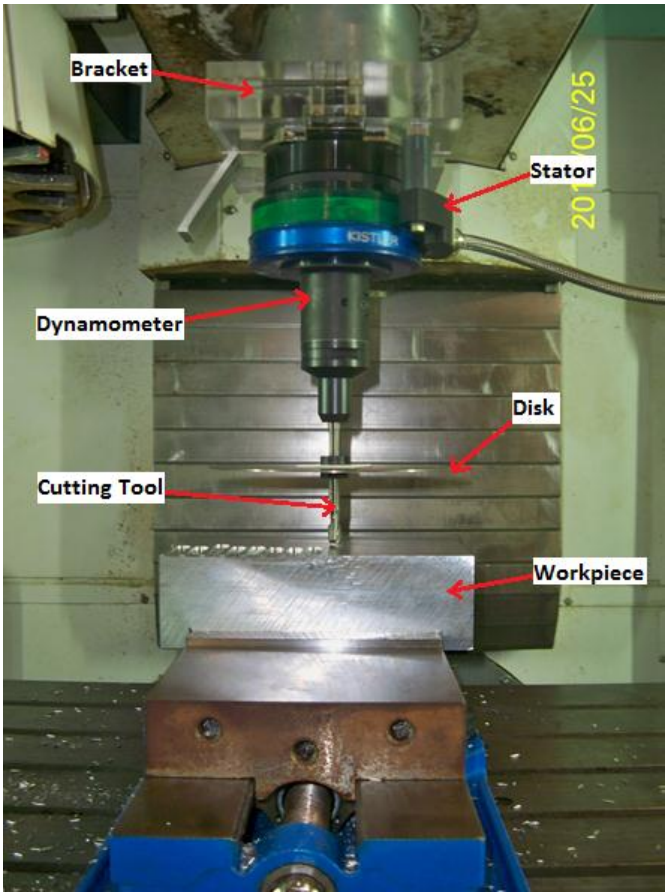

Figure 28: Experimental setup for dynamometer to determine the cutting forces with the disc attached to the cutting tool.

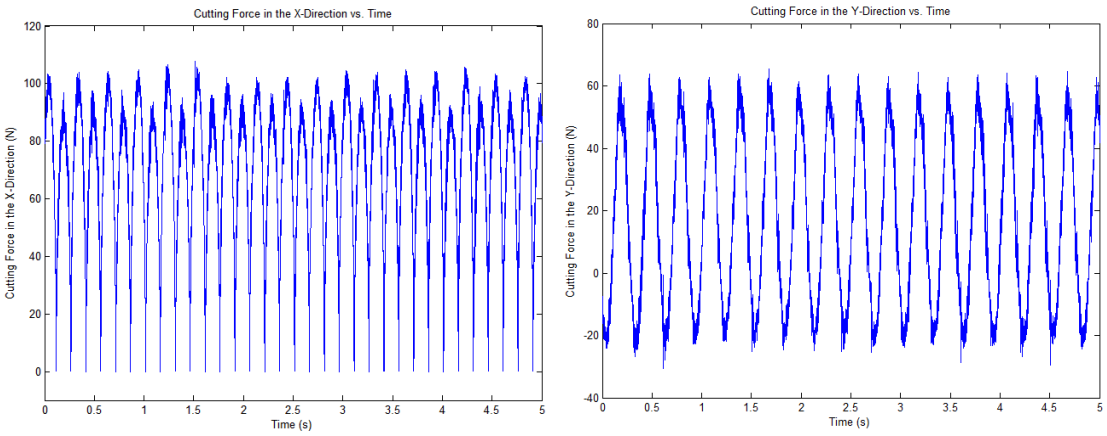

Figure 29: Slot milling cut was made at 2 mm depth of cut, spindle speed of 200 rpm, and a feed rate of 0.05 mm/rev. Cutting Forces in the x and y direction for the cutting tool with the disc.

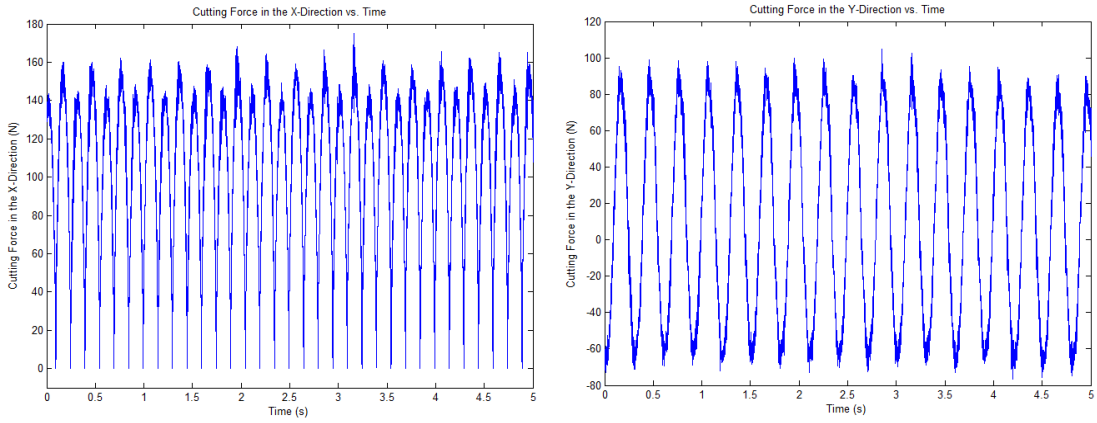

Figure 30: Slot milling cut was made at 2 mm depth of cut, spindle speed of 200 rpm, and a feed rate of 0.10 mm/rev. Cutting Forces in the x and y direction for the cutting tool with the disc.

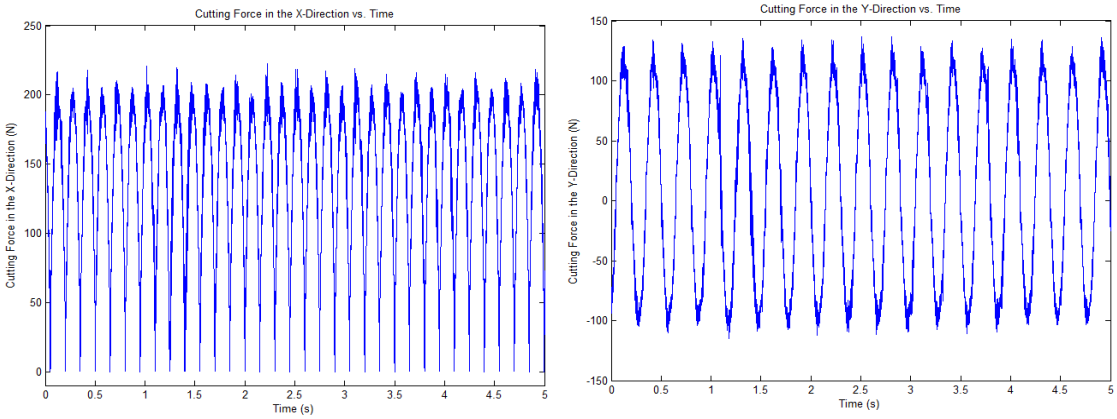

Figure 31: Slot milling cut was made at 2 mm depth of cut, spindle speed of 200 rpm, and a feed rate of 0.15 mm/rev. Cutting Forces in the x and y direction for the cutting tool with the disc.

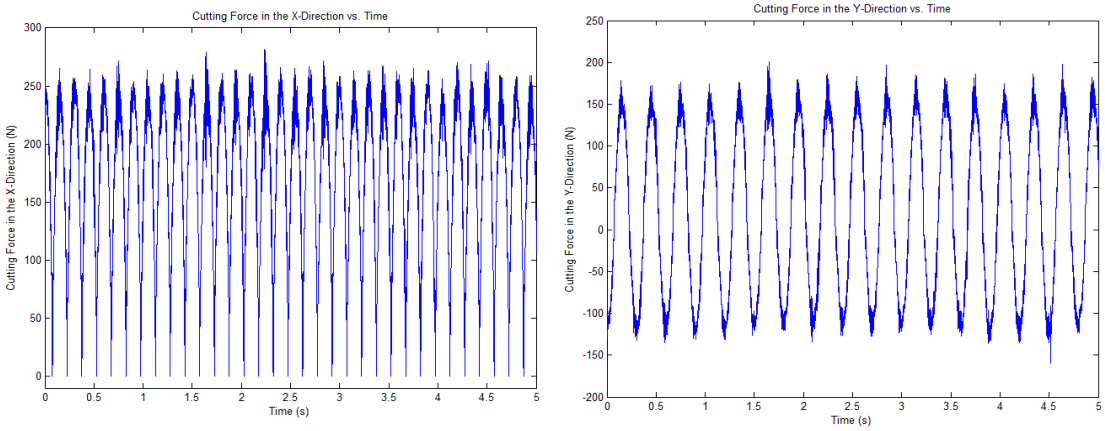

Figure 32: Slot milling cut was made at 2 mm depth of cut, spindle speed of 200 rpm, and a feed rate of 0.20 mm/rev. Cutting Forces in the x and y direction for the cutting tool with the disc.

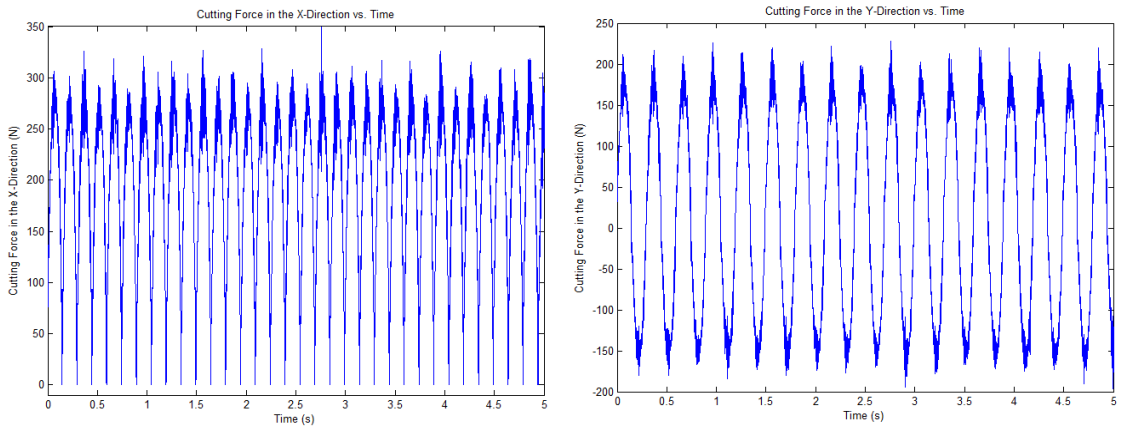

Figure 33: Slot milling cut was made at 2 mm depth of cut, spindle speed of 200 rpm, and a feed rate of 0.25 mm/rev. Cutting Forces in the x and y direction for the cutting tool with the disc.

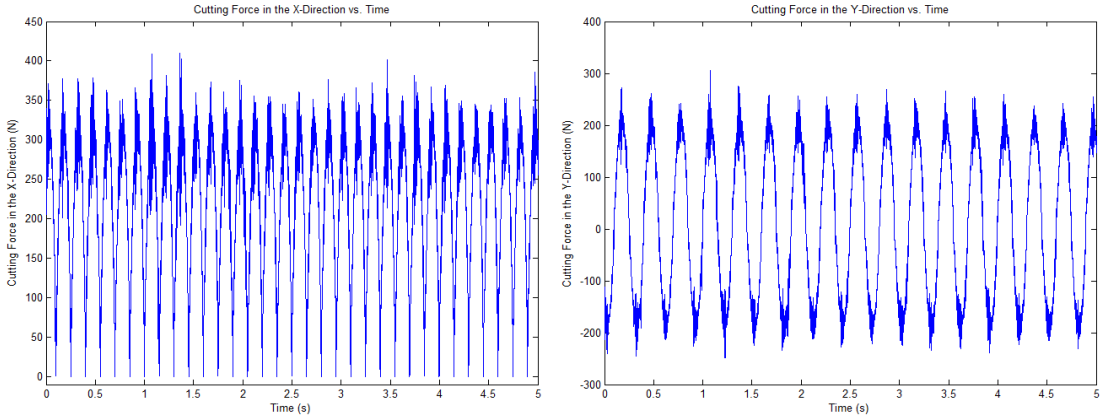

Figure 34: Slot milling cut was made at 2 mm depth of cut, spindle speed of 200 rpm, and a feed rate of 0.30 mm/rev. Cutting Forces in the x and y direction for the cutting tool with the disc.

5.4: Comparison of Cutting Forces for the Cutting Tool with and without the Thin Disc Attached

From Table 2, it's clear that the addition of the disc slightly increased the cutting forces in the *x* and *y* direction. This may be attributed to the additional mass of the disc on the cutting tool. The mass of the disc may not have been completely balanced around the cutting tool neck due to the tool run out and assembly error.

The increase of the cutting forces in the *x* and *y* direction may increase the displacement of the cutting tool. Therefore, any experimental results measuring the

displacement of the disc in the *z* direction may be greater than the theoretical displacements of the disc if the disc was assumed to have no effect on the cutting tool mechanics.

Table 2: Maximum cutting force acting on the tool in the x and y direction with and without the disc attached to the tool for the six different feed rates.

Feed Rate	**Px Maximum (without disc)**	**Px Maximum (with disc)**	**% Change**
0.05 mm/rev	92.2 N	97.6 N	+5.857 %
0.10 mm/rev	146.5 N	148.3 N	+1.16 %
0.15 mm/rev	198.9 N	209.8 N	+5.48 %
0.20 mm/rev	247.7 N	253.2 N	+2.222 %
0.25 mm/rev	285.7 N	294.8 N	+3.185 %
0.30 mm/rev	358.0 N	363.5 N	+1.536 %
Feed Rate	**Py Maximum (without disc)**	**Py Maximum (with disc)**	**% Change**
0.05 mm/rev	53.0 N	59.7 N	+12.64 %
0.10 mm/rev	88.3 N	93.6 N	+6.002 %
0.15 mm/rev	121.9 N	127.2 N	+4.348 %
0.20 mm/rev	167.8 N	178.4 N	+6.317 %
0.25 mm/rev	183.7 N	197.9 N	+7.73 %
0.30 mm/rev	229.7 N	249.1 N	+8.466 %

Chapter 6: Verification of FEA Method

In this Chapter, the FEA method used to determine the stress and displacement of the cutting tool during chatter from Chapter 3 is verified. To confirm that the results obtained from the FEA simulation are accurate, Solidworks simulations are performed for the experimental slot milling cuts described in Section 5.3.1. To run the simulations, the cutting forces data for the cutting tool without the disc in Section 5.3.1 are inputted for the forces applied on the cutting edge of the tool model. The Solidworks simulation setup and results can be found in Section 6.1. To verify that the FEA displacements of the cutting tool during the slot milling cuts are accurate, the slot milling cuts are redone using the previous tool displacement measurement system described in Chapter 2. The procedure and results for measuring the tool displacements using the previous tool displacement measurement method can be found in Section 6.2. The verification of the FEA results can be found in Section 6.3. The FEA simulations using the cutting forces of the cutting tool with the disc from Section 5.3.2 can be found in Section 6.4.

6.1: Solidworks Tool Displacement Simulation Using Tool Cutting Forces

The same 3D model of the cutting tool from Section 3.2 was used for this simulation. However the small extruded cut made on the cutting edge of the tool was moved down from 3.55 mm to 2 mm to match the depth of cut for the slot milling cuts. Since more data points were collected by the dynamometer per revolution, the simulation ran for only two cutting tool revolutions. To save running time on the simulation, only 20 cutting force data points were selected at even intervals over the two tool revolutions.

The top of the cutting tool was fixed in the same manner used for the chatter simulation as described in Section 3.4. The circumferential translation was set from 0 to 12.566 rad since the simulation ran for only two tool revolutions. The 20 x and y forces were selected from the cutting forces in the fixed and y direction found experimentally in Section 5.3.1. The

maximum displacements in the x and y direction of the tracker on the cutting tool neck were recorded (see Table 3).

Table 3: Maximum displacements of the tracker in the x and y direction for the cutting tool simulation using the cutting forces as the applied force on the cutting edge of the tool.

Feed Rate (mm/rev)	Maximum x direction displacement (mm)	Maximum x direction displacement (mm)
0.05	0.0476 mm	0.0405 mm
0.10	0.0806 mm	0.0568 mm
0.15	0.1233 mm	0.0834 mm
0.20	0.1537 mm	0.1095 mm
0.25	0.1842 mm	0.1294 mm
0.30	0.2116 mm	0.1489 mm

6.2: Cutting Tool Displacement Found Using Previous Tool Displacement Measurement Method

The previous tool displacement measurement setup described in Chapter 2 is assembled. The procedure for the calibration of the capacitive sensors can be found in appendix B. The calibration constants were found to be 10.1874 V/mm for the capacitive sensor in the x direction and 10.9206 V/mm for the capacitive sensor in the y direction. The Aluminum 6061 T-6511 workpiece was placed with the longest direction in the horizontal direction into the vice and the vice was clamped tight to secure the workpiece. The same experimental slot milling cuts described in Section 5.3.1 were performed to obtain the data for the displacements in x and y direction (see Figures 35-40).

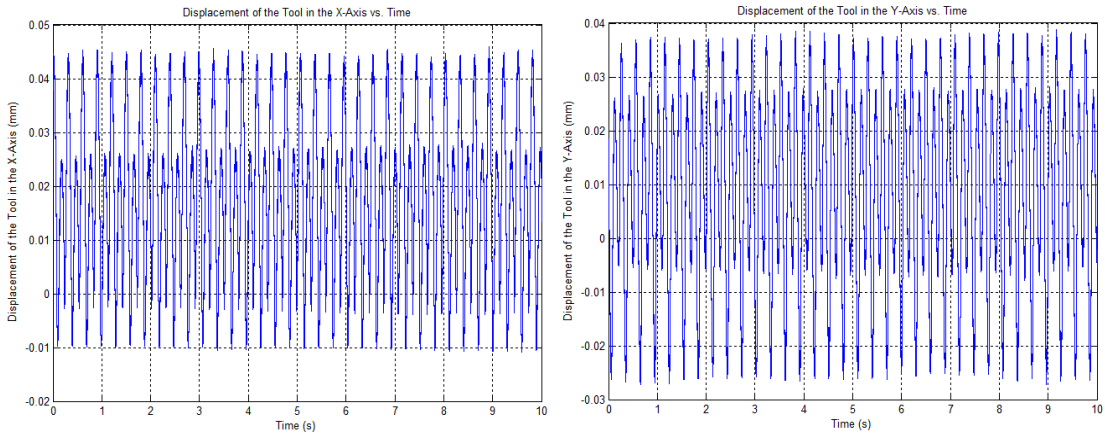

Figure 35: Displacements of the cutting tool in the x and y-direction for a slot milling cut with 2 mm depth of cut, spindle speed of 200 rpm, and feed rate of 0.05 mm/rev.

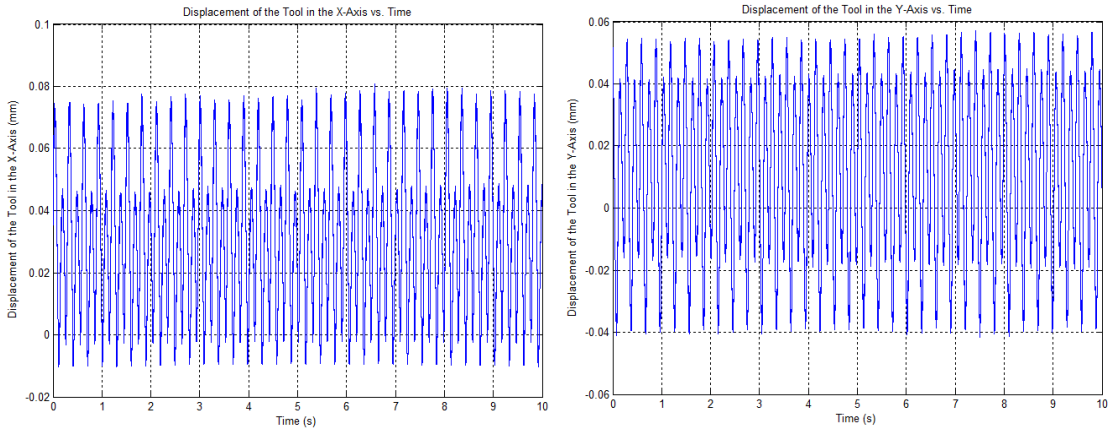

Figure 36: Displacements of the cutting tool in the x and y-direction for a slot milling cut with 2 mm depth of cut, spindle speed of 200 rpm, and feed rate of 0.10 mm/rev.

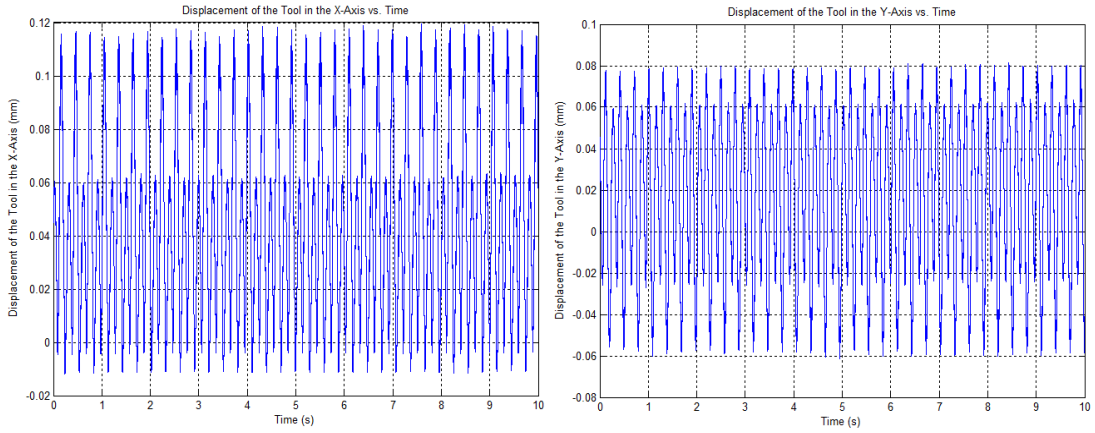

Figure 37: Displacements of the cutting tool in the x and y-direction for a slot milling cut with 2 mm depth of cut, spindle speed of 200 rpm, and feed rate of 0.15 mm/rev.

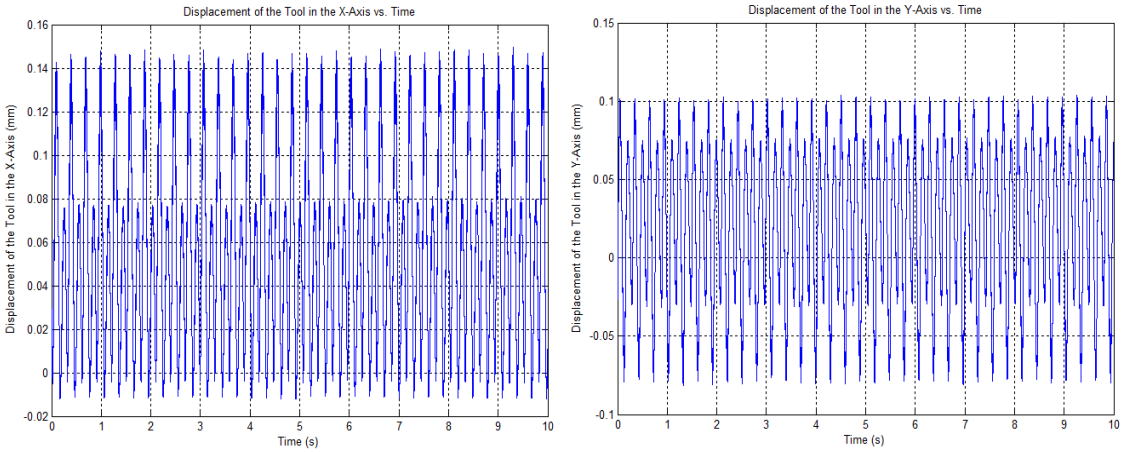

Figure 38: Displacements of the cutting tool in the x and y-direction for a slot milling cut with 2 mm depth of cut, spindle speed of 200 rpm, and feed rate of 0.20 mm/rev.

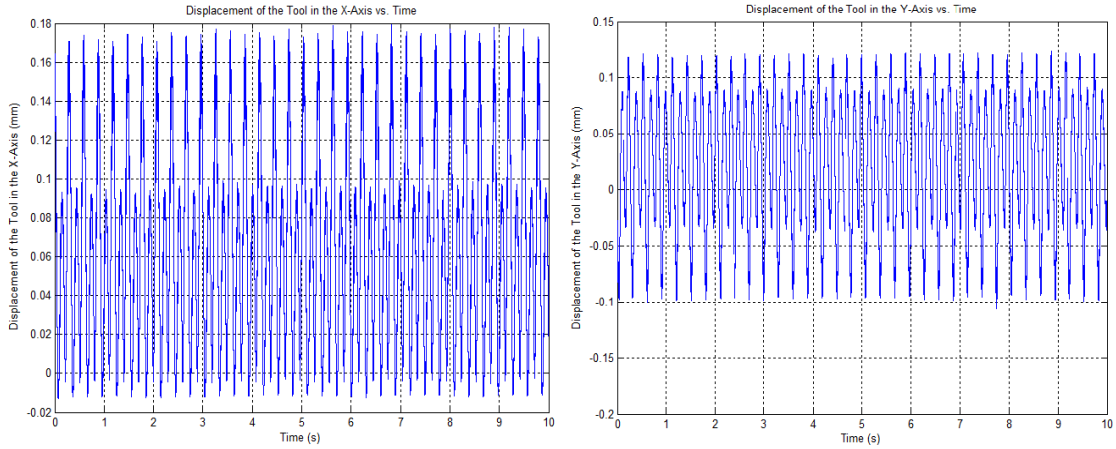

Figure 39: Displacements of the cutting tool in the x and y-direction for a slot milling cut with 2 mm depth of cut, spindle speed of 200 rpm, and feed rate of 0.25 mm/rev.

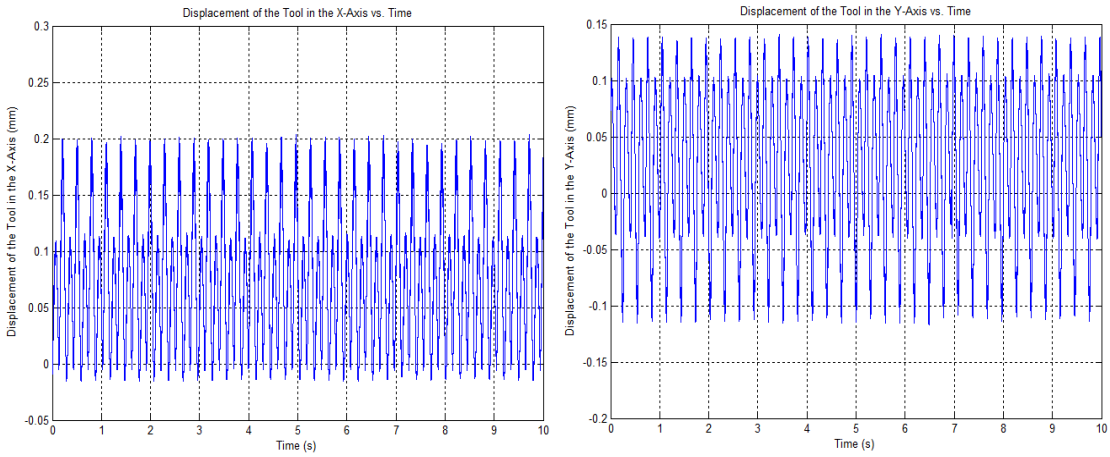

Figure 40: Displacements of the cutting tool in the x and y-direction for a slot milling cut with 2 mm depth of cut, spindle speed of 200 rpm, and feed rate of 0.30 mm/rev.

6.3: Verification of FEA Simulation Results

To verify that the results from the Solidworks simulations are accurate, the maximum displacements of the cutting tool in the x and y direction found by the simulation are compared to the maximum displacements of the cutting tool in the x and y direction measured experimentally. The percent error between the two methods for each feed rate was evaluated to observe the accuracy of the FEA method (see Tables 4 and 5).

Table 4: Comparison of Solidworks simulations and experimental results for the maximum displacement of the cutting tool in the x direction 1.75 in from the bottom of the tool.

Feed Rate (mm/rev)	Max Displacement in the X direction (Simulation)	Max Displacement in the X direction (Experimental)	Error %
0.05	0.0476 mm	0.0448 mm	6.25 %
0.10	0.0806 mm	0.0773 mm	4.27 %
0.15	0.1233 mm	0.1184 mm	4.14 %
0.20	0.1537 mm	0.1452 mm	5.85 %
0.25	0.1842 mm	0.1775 mm	3.78%
0.30	0.2116 mm	0.2003 mm	5.64%

Table 5: Comparison of Solidworks simulations and experimental results for the maximum displacement of the cutting tool in the y direction 1.75 in from the bottom of the tool.

Feed Rate (mm/rev)	Max Displacement in the Y direction (Simulation)	Max Displacement in the Y direction (Experimental)	Error %
0.05	0.0405 mm	0.0378 mm	7.14%
0.10	0.0568 mm	0.0534 mm	6.37%
0.15	0.0834 mm	0.0799 mm	4.38%
0.20	0.1095 mm	0.1041 mm	5.19%
0.25	0.1294 mm	0.1217 mm	6.33%
0.30	0.1489 mm	0.1408 mm	5.75%

From the comparisons made in Tables 4 and 5, it is clear that the Solidworks Simulation was accurate in its method of determining the displacement of the cutting tool given the cutting forces. Overall, the simulation had a +4.99% error for the maximum displacements in the x direction and +5.87% error for the maximum displacement in the y direction. This error that resulted greater displacements in the Solidworks simulation could be attributed to multiple factors.

One factor could be that the geometry for the 3D model of the cutting tool may not have been %100 accurate. Another factor could be that Tungsten Carbide is a ceramic material and is very brittle. Very brittle materials create a problem for finding accurate material properties, so the Young's modulus for Tungsten Carbide ranges from 668.17 GPa to 713.61 GPa [24]. For the Solidworks simulations, the young's modulus used was 680 GPa, so the large range of the Young's modulus could easily account for the 5% error found in the displacements. Another factor could be that the measurement of the cutting forces found by the dynamometer or the displacement measured by the previous tool displacement measurement method may not have been %100 accurate.

Since the 5% error can be accounted for, the Solidworks simulation was found to be accurate and is a good representation of the tool displacement while undergoing a milling operation.

6.4: FEA Tool Displacement Simulation Using Cutting Forces of Tool with Disc

The Solidworks simulation was ran again with the cutting forces of the tool with the disc attached as the applied force on the cutting edge. The increase in force created a small increase in the maximum displacement in the x and y direction (see Tables 3 and 6).

Table 6: Maximum displacements of the tracker in the x and y direction for the cutting tool simulation using the cutting forces for the cutting tool with the disc as the applied force on the cutting edge of the tool.

Feed Rate (mm/rev)	Maximum X-direction Displacement (mm)	Maximum Y-direction Displacement (mm)
0.05	0.0474 mm	0.0426 mm
0.10	0.0782 mm	0.0566 mm
0.15	0.1248 mm	0.0834 mm
0.20	0.1484 mm	0.1107 mm
0.25	0.1832 mm	0.1311 mm
0.30	0.2034 mm	0.1527 mm

Chapter 7: New Tool Concept Validation

In this Chapter, the proof of concept for the new tool's ability to indirectly measure the displacement in the cutting tool is validated. An experiment is designed to employ the experimental new cutting tool and measure the displacement of the disc in the z direction while the slot milling cuts described in Section 5.3.1 are performed. The experimental setup of the new tool design validation experiment can be found in Section 7.1. The experimental procedure for the new tool design validation experiment can be found in Section 7.2. The results for the new tool design validation experiment can be found in Section 7.3. The conclusion of the new tool design validation can be found in Section 7.4.

7.1: Experimental Setup for New Tool Validation

The experimental tool with disc described in Section 4.4 is inserted into the tool holder and secured in place. To measure the displacement of the disc in the z direction, a new sensor holder that holds the capacitive displacement sensors vertical was created. The design of the sensor holder began by drawing a vertical sensor holder half in Solidworks (see Figure 41).

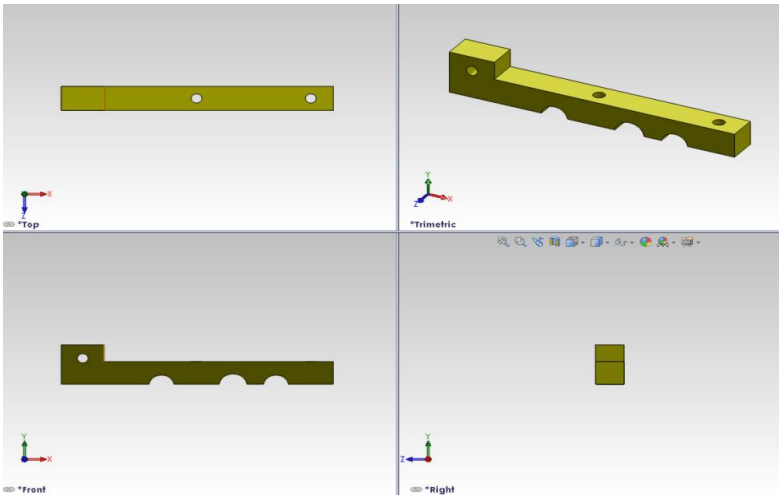

Figure 41: Top, front, side, and trimetric view of vertical sensor holder half. Part was modeled in Solidworks and saved as a .stl file and fabricated using a fused deposition modeling machine.

Two vertical holder halves were needed for each the x and y direction capacitive displacement sensor. A total of four vertical holder halves were fabricated using a fused deposition modeling machine. Each pair of vertical sensor holder halves was attached to a slanted metal piece using screws. A slot and two holes by the x and y axis on the mounting bracket allowed the slanted metal pieces to connect to the mounting bracket using screws. The slanted metal pieces were centered along the x and y axis of the CNC machine which positioned the capacitive sensors on the x and y axis of the CNC machine (see Figure 42).

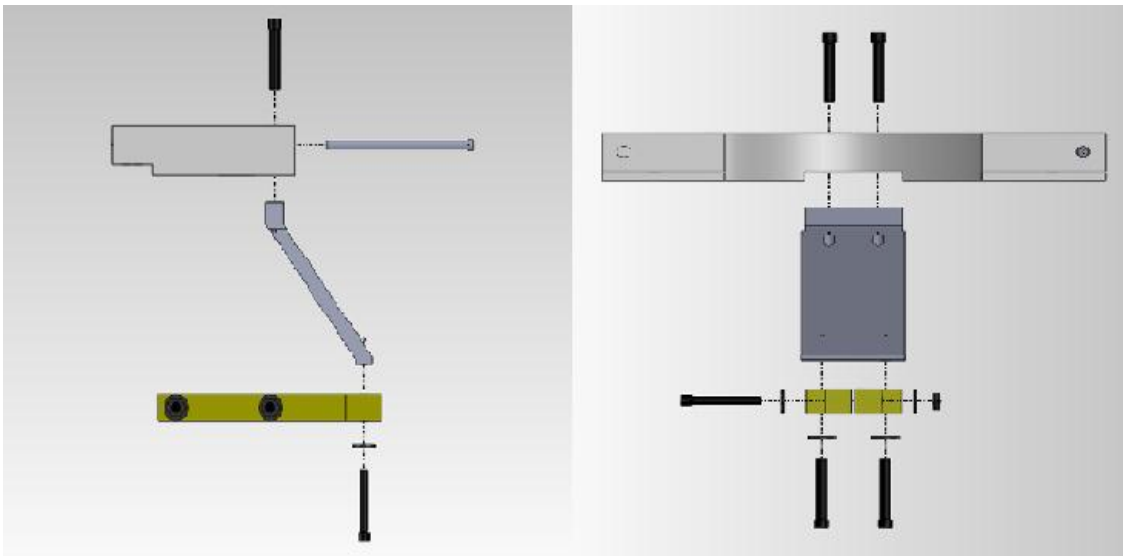

Figure 42: Exploded front view of the vertical sensor setup (left). Exploded side view of the vertical sensor setup (right).

To secure the sensors in the vertical position, the vertical sensor holder halves will be clamped together using screws. This vice-like design allows the capacitance sensors' height to be adjusted easily. An assembly drawing of the entire experimental setup was created in Solidworks so interference between parts can be automatically checked [18] (see Figure 43).

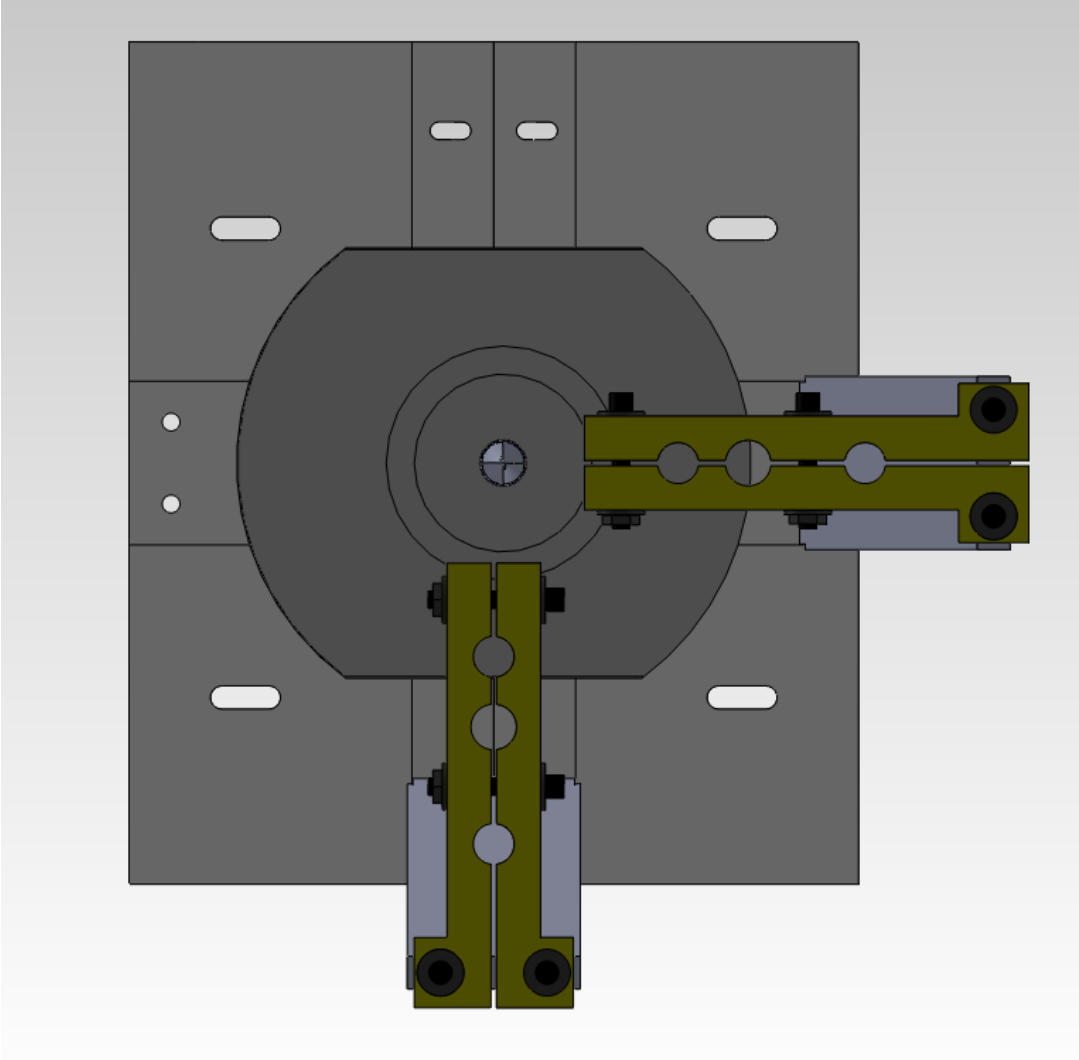

Figure 43: Bottom view of vertical sensor holder setup without sensors in place. Screws/Nuts are tightened to clamp sensors in between the two vertical sensor holder halves.

Once the interferences were corrected, the vertical holder halves were fabricated using a fused deposition modeling machine and the assembly was constructed on the CNC machine. The same DAC system that was used in the previous tool displacement measurement method was utilized to receive the signal from the capacitive sensors. The procedure for the calibration of the capacitive sensors can be found in appendix B. The calibration constants were found to be 10.1874 V/mm for the capacitive sensor above the x axis of the disc and 10.9206 V/mm for the capacitive sensor above the y axis of the disc.

7.2: Experimental Procedure for New Tool Design Validation

The experimental setup was assembled with the disc at a height of 1.75 in from the cutting tool tip. With the disc at the lower position on the tool neck, the capacitive sensors were placed in the closest sensor holder located 2.25 in away from the cutting tool. The height of the capacitance sensors was set so that the distance readings were approximately in the center of the distance measurement range of the capacitance sensor. The tachometer was placed in the center sensor holder of the vertical sensor holder. A small piece of non-reflective tape was placed on the thin disc at the same distance away from the cutting tool as the tachometer (see Figure 44).

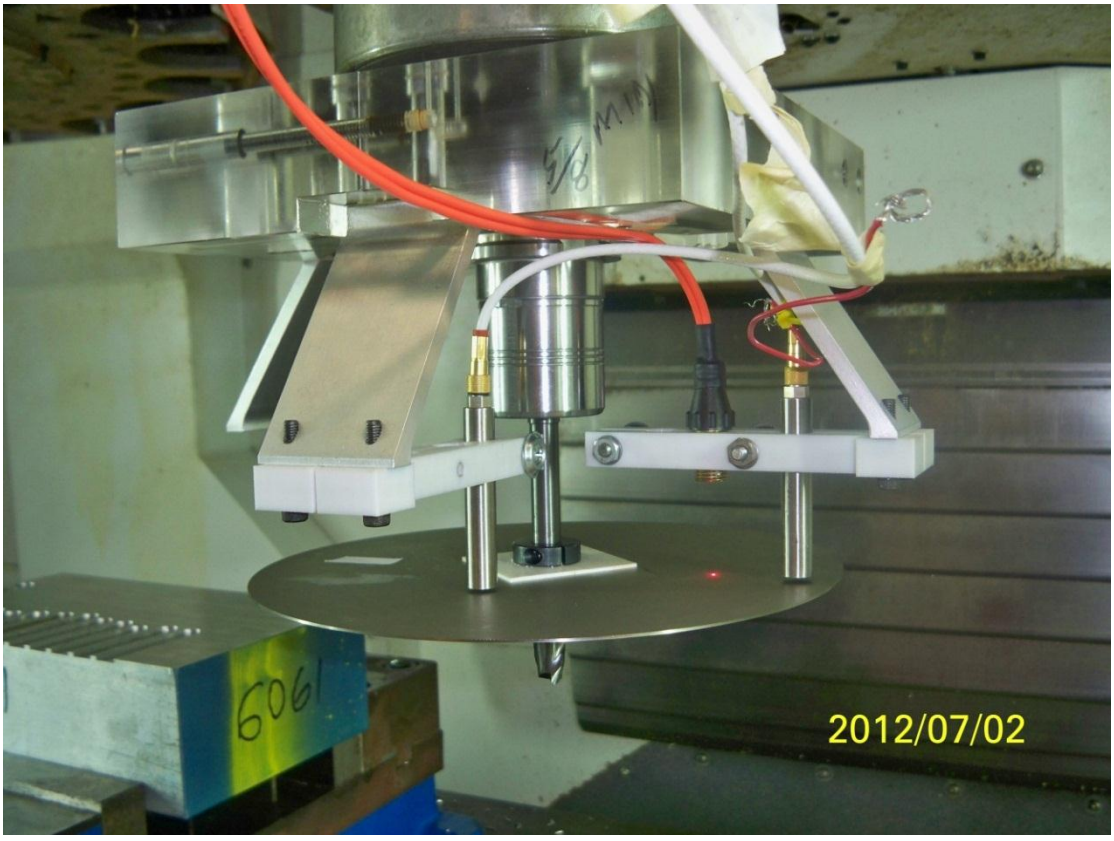

Figure 44: Vertical sensor holder assembly with capacitance sensors and tachometer setup. Thin disc is attached to the cutting tool and non-reflective tape was placed on the disc.

As the disc rotates with the cutting tool, the laser being reflected back to tachometer would be disrupted at each pass of the non-reflective tape on the disc. The on and off laser signal received by the tachometer would go back and forth creating a square wave. The frequency of the square wave is then calculated by the tachometer and is outputted as the rpm of the disc.

The tachometer also allows the orientation of the disc to be determined from the collected data. The knowledge of when a disc revolution begins and ends allows for a profile of the disc height to be created from the capacitive displacement sensor data. Since the disc was manufactured in the machine lab, it may not have been perfectly flat or level on the cutting tool. A profile of the disc height as it rotates is critical to obtaining the displacements of the disc in the *z* direction during a milling operation. The profile of the disc was created with the experimental new cutting tool rotating at 200 rpm and not cutting. The speed of 200 rpm was chosen so that the profile can easily be aligned and subtracted from the slot milling cuts performed in the experiment. Therefore, the actual disc displacement in the *z* direction due to the tool displacement can be determined relative to the displacements that are due to the profile of the disc while not cutting.

The same slot milling cuts that were described in Section 5.3.1 were performed with the experimental new tool design and vertical sensor assembly.

7.3: Experimental Results for New Tool Design Validation

The profile of the disc height in the *z* direction was aligned with the disc displacement data using the tachometer signal and subtracted from the disc displacement data for both the *x* and *y* axis sensors for each of the 6 slot milling cuts. The resulting data was plotted and illustrates the disc displacement in the z direction above the *x* and *y* axis due to the cutting tool

displacement. The measured disc displacement in the *z* direction above the *x* and *y* axis due to the tool displacement for each of the six different feed rates can be observed in Figures 45-50.

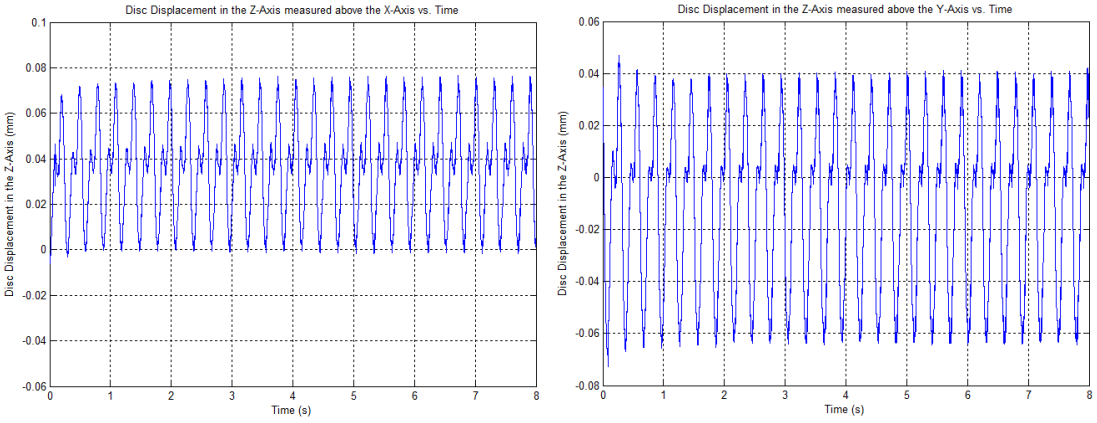

Figure 45: Disc Displacement in the z-direction measured above the x and y-axis for the slot milling cut with a depth of cut of 2 mm, spindle speed of 200 rpm, and a feed rate of 0.05 mm/rev.

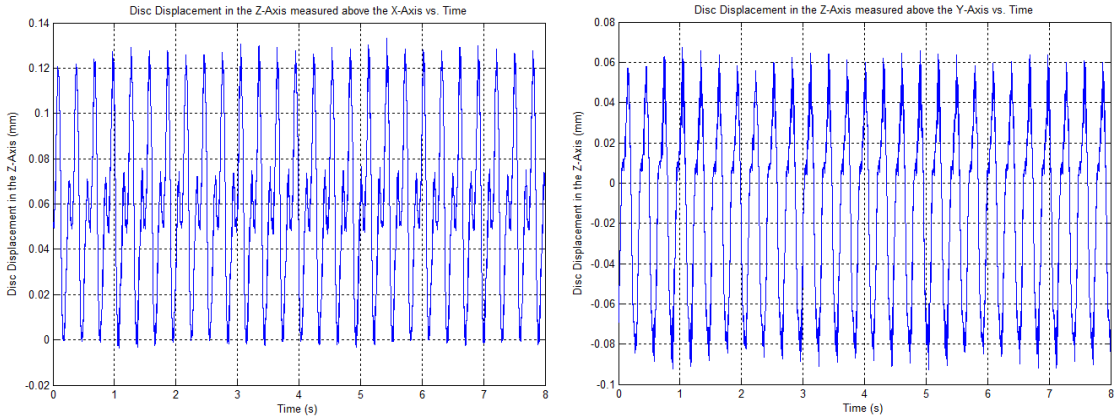

Figure 46: Disc Displacement in the z-direction measured above the x and y-axis for the slot milling cut with a depth of cut of 2 mm, spindle speed of 200 rpm, and a feed rate of 0.10 mm/rev.

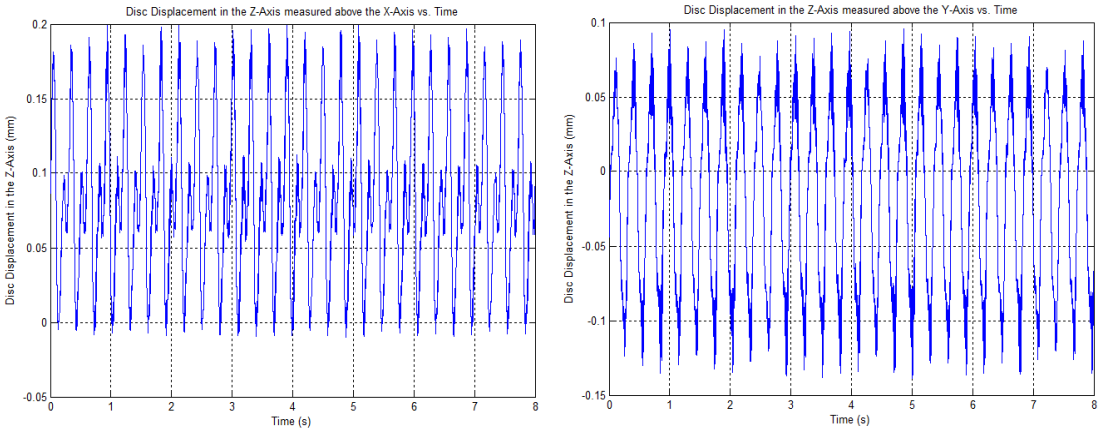

Figure 47: Disc Displacement in the z-direction measured above the x and y-axis for the slot milling cut with a depth of cut of 2 mm, spindle speed of 200 rpm, and a feed rate of 0.15 mm/rev.

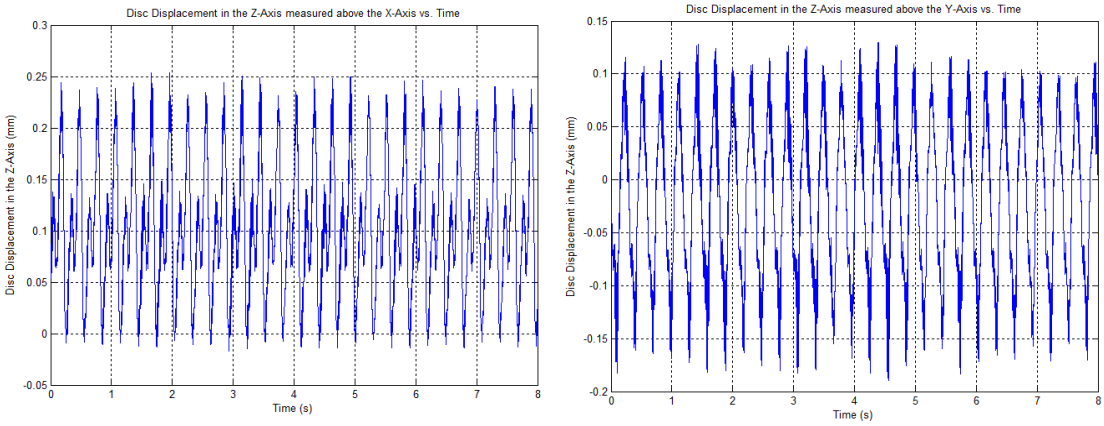

Figure 48: Disc Displacement in the z-direction measured above the x and y-axis for the slot milling cut with a depth of cut of 2 mm, spindle speed of 200 rpm, and a feed rate of 0.20 mm/rev.

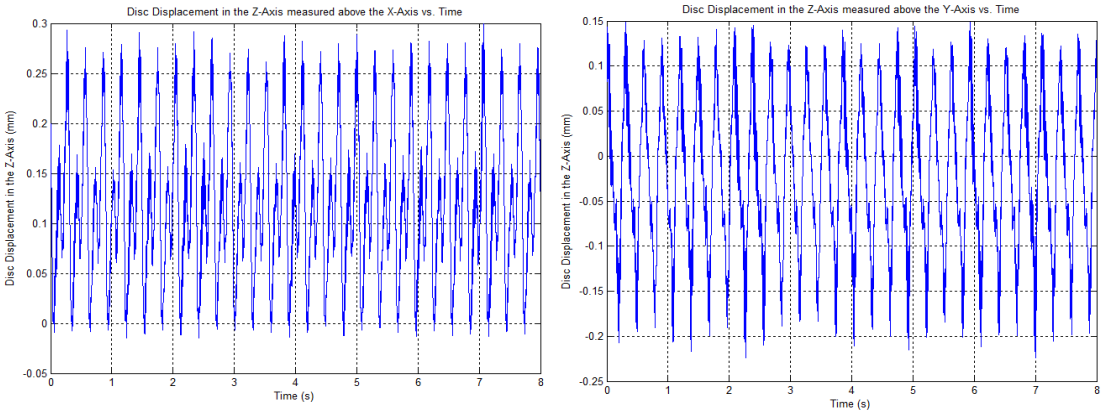

Figure 49: Disc Displacement in the z-direction measured above the x and y-axis for the slot milling cut with a depth of cut of 2 mm, spindle speed of 200 rpm, and a feed rate of 0.25 mm/rev.

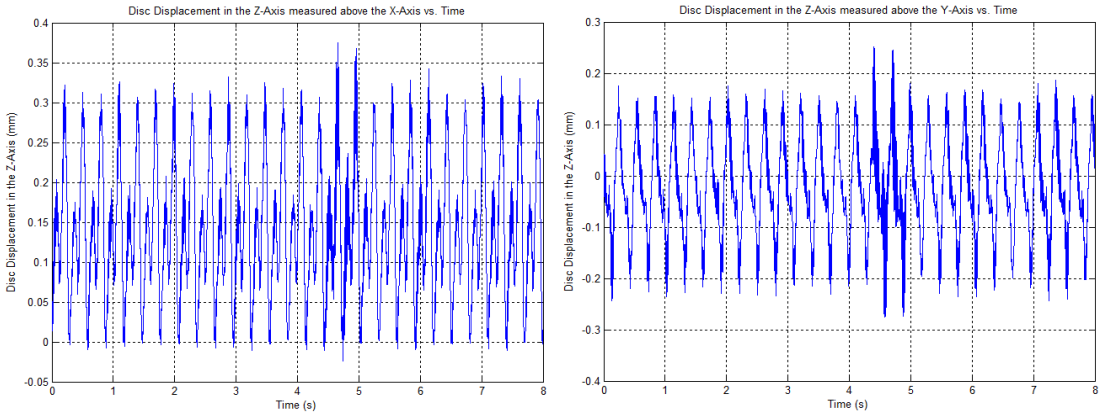

Figure 50: Disc Displacement in the z-direction measured above the x and y-axis for the slot milling cut with a depth of cut of 2 mm, spindle speed of 200 rpm, and a feed rate of 0.30 mm/rev.

7.4: Conclusion of New Tool Design Validation

To validate the new tool design, the experiment needs to provide proof that the new tool design is able to indirectly measure the displacement of the cutting tool. The tool displacements in the *x* and *y* direction were derived from the disc displacements in the z direction above the *x* and *y* axis respectively using Equations 20 and 21.

To verify that the new tool design measures the displacement of the cutting tool accurately, the maximum tool displacements derived from the maximum disc displacements are compared to the maximum tool displacements found by two alternative methods for determining tool displacement.

One of the alternative methods was the prior sensor housing tool displacement measurement method. Since the disc can't be attached onto the cutting tool with the previous tool displacement measurement assembly attached to the spindle, the measured tool displacements without the disc from Section 6.2 are used as an approximation for the comparison. The other alternative method was the FEA tool displacement simulation method. For this comparison, the FEA simulations using the cutting forces for the tool with the disc from Section 6.4 were utilized.

The maximum displacements in the *x* and *y* direction using the three different methods can be found in Tables 7 and 8 respectively.

Table 7: Comparison of the maximum tool displacement in the x direction found by the new tool design method, the prior displacement sensor housing assembly, and by FEA simulation.

Feed rate (mm/rev)	Maximum disc displacement above x axis	New tool design method maximum tool displacement in x direction	Prior measurement method maximum tool displacement in x direction	FEA maximum tool displacement in the x direction
0.05	0.0756 mm	0.0478 mm	0.0448 mm	0.0474 mm
0.10	0.1282 mm	0.0811 mm	0.0773 mm	0.0782 mm
0.15	0.1965 mm	0.1243 mm	0.1184 mm	0.1248 mm
0.20	0.2414 mm	0.1527 mm	0.1452 mm	0.1484 mm
0.25	0.2891 mm	0.1829 mm	0.1775 mm	0.1832 mm
0.30	0.3279 mm	0.2075 mm	0.2003 mm	0.2034 mm

Table 8: Comparison of the maximum tool displacement in the y direction found by the new tool design method, the prior displacement sensor housing assembly, and by FEA simulation.

Feed rate (mm/rev)	Maximum disc displacement above y axis	New tool design method maximum tool displacement in y direction	Prior measurement method maximum tool displacement in y direction	FEA maximum tool displacement in the y direction
0.05	0.0639 mm	0.0404 mm	0.0378 mm	0.0426 mm
0.10	0.0896 mm	0.0567 mm	0.0534 mm	0.0566 mm
0.15	0.1336 mm	0.0845 mm	0.0799 mm	0.0834 mm
0.20	0.1711 mm	0.1082 mm	0.1041 mm	0.1107 mm
0.25	0.2003 mm	0.1267 mm	0.1217 mm	0.1311 mm
0.30	0.2315 mm	0.1465 mm	0.1408 mm	0.1527 mm

The maximum displacements in the *x* and *y* direction were relatively close between the three different methods. The percent error between the new tool design method and the other two methods was calculated. The percent error for the maximum tool displacement in the x and y direction can be found in Tables 9 and 10 respectively.

Table 9: Percent error of the maximum tool displacement in the x direction between the new tool design method and the prior displacement sensor housing method, and between the new tool design method and the FEA simulation.

Feed Rate (mm/rev)	% Error between max tool displacement in x from disc and max tool displacement in x from prior displacement measurement setup	% Error between max tool displacement in x from disc and max tool displacement in x from FEA
0.05	6.696 %	0.844 %
0.10	4.196 %	3.708 %
0.15	4.983 %	-0.400 %
0.20	5.165 %	2.898 %
0.25	3.042 %	-0.164 %
0.30	3.595 %	2.016 %

Table 10: Percent error of the maximum tool displacement in the y direction between the new tool design method and the prior displacement sensor housing method, and between the new tool design method and the FEA simulation.

Feed Rate (mm/rev)	% Error between max tool displacement in y from disc and max tool displacement in y from prior displacement measurement setup	% Error between max tool displacement in y from disc and max tool displacement in y from FEA
0.05	6.878 %	-5.164 %
0.10	6.180 %	0.177 %
0.15	5.757 %	1.319 %
0.20	3.939 %	-2.258 %
0.25	4.108 %	-3.356 %
0.30	4.048 %	-4.060 %

From Tables 9 and 10, it's clear that the new tool design method for measuring the tool displacement is accurate. A graphical comparison of the results from the three different displacement measurement methods of the tool in the *x* and *y* direction for 0.05 mm/rev can be seen in Figures 51 and 52 respectively.

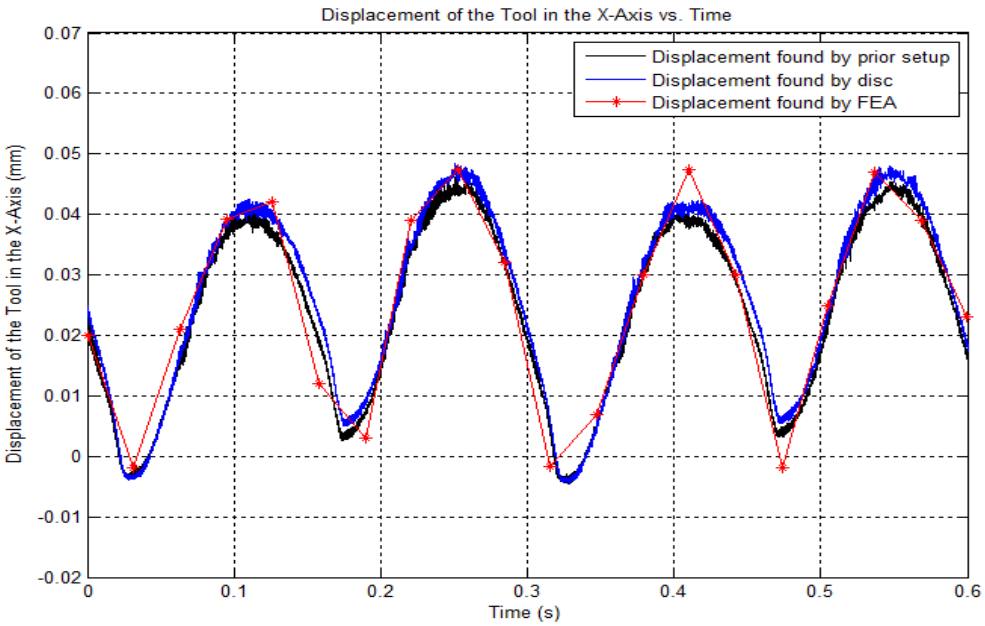

Figure 51: Graphical comparison of the results from three different displacement measurement methods for the displacement of the tool in the *x* direction for a feed rate of 0.05 mm/rev.

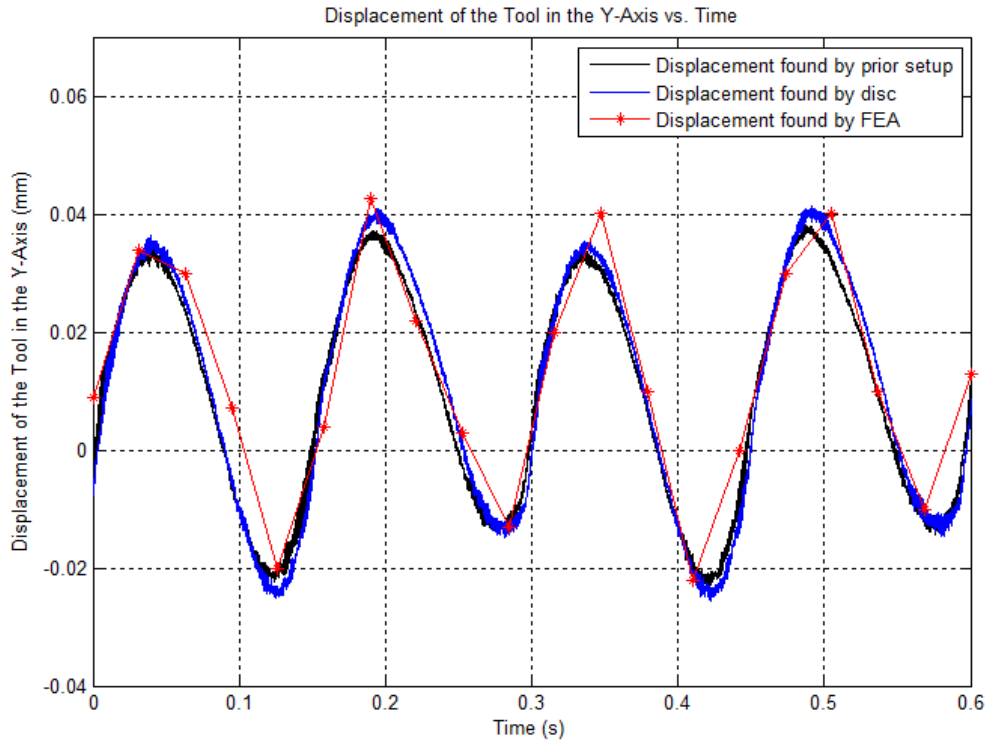

Figure 52: Graphical comparison of the results from three different displacement measurement methods for the displacement of the tool in the *y* direction for a feed rate of 0.05 mm/rev.

The small percentage error between the methods could be attributed to multiple reasons. The main reason that the displacement results found by the FEA method is jagged and inaccurate as seen in Figures 51 and 52 is due to the small number of data points. A greater number of data points in the FEA method would have created a smoother and more accurate result. The main reason for the small percentage error between the tool displacement measured by the new tool design and the prior measurement method was that it was impossible to simultaneously have the capacitance sensors measuring the neck of the tool while the disc is attached at the same height. The added weight and higher cutting forces due to the addition of the disc could easily explain for the difference between the measured tool displacements.

There are several reasons for the small percentage error between the tool displacement measured by the new tool design method and the FEA method. First of all, the FEA method may not be %100 accurate in determining the tool displacements as discussed in Section 6.3. Another reason is although the higher cutting forces were used in the simulation, the disc was not a part of the 3D model. Even though the disc was not actually part of the tool, the disc and clamp collars had an influence on the tool displacement.

Chapter 8: Future Work and Conclusion

8.1: Ideal Experimental Setup for Future Research

The validation of the new tool design method for indirectly measuring the displacement in the cutting tool enables future research to be performed on this topic. Several Improvements to the experimental setup can be made. First of all, the cutting tool with the disc can be manufactured with the disc as part of the cutting tool. Having the disc directly connected to the cutting tool would ensure that the disc is completely flat, and the tilt of the disc will exactly reflect the curvature in the tool while under stress.

The disc being connected to the cutting tool also allows for numerous other experiments to be performed. The model parameter estimates of the new cutting tool design (i.e. modal mass, stiffness, and damping) can be determined. This can be achieved by performing a static load test to find the stiffness coefficient and a dynamic model test using an impact hammer and accelerometer to find the modal mass and damping coefficient. Once estimates of the model parameters are known, simulations of the dynamics for a given milling operation with the new tool design can be performed [13].

For the research presented in this paper, the milling cuts were performed at low spindle speeds to guarantee that the disc stayed securely attached to the cutting tool. A manufactured new tool with the disc connected would allow for high speed milling experiments to be conducted.

Another modification to the experimental setup would be better displacement sensors. For the research presented in this paper, the capacitive displacement sensors were employed because of their availability. The constraints on the capacitive sensors such as the range of

measurement and requirement of measuring a conductive target made the experiment have limited freedom in design. A better suited choice given the availability would have been a laser displacement sensor. The laser displacement sensor has a much broader range of measurement allowing it to be attached to the spindle or other locations on the CNC machine. The laser displacement sensor could also measure any type of material which would allow more choices for the material of the thin disc such as lightweight plastics. Also, the laser displacement sensors run at very high frequencies allowing for the testing of high speed milling operations.

Overall the experiment performed on the new tool design presented in this paper was adequate. But with the manufactured new cutting tool with disc and the laser displacement sensor, the experiment would have a lot more freedom with more accurate results (see Figure 53).

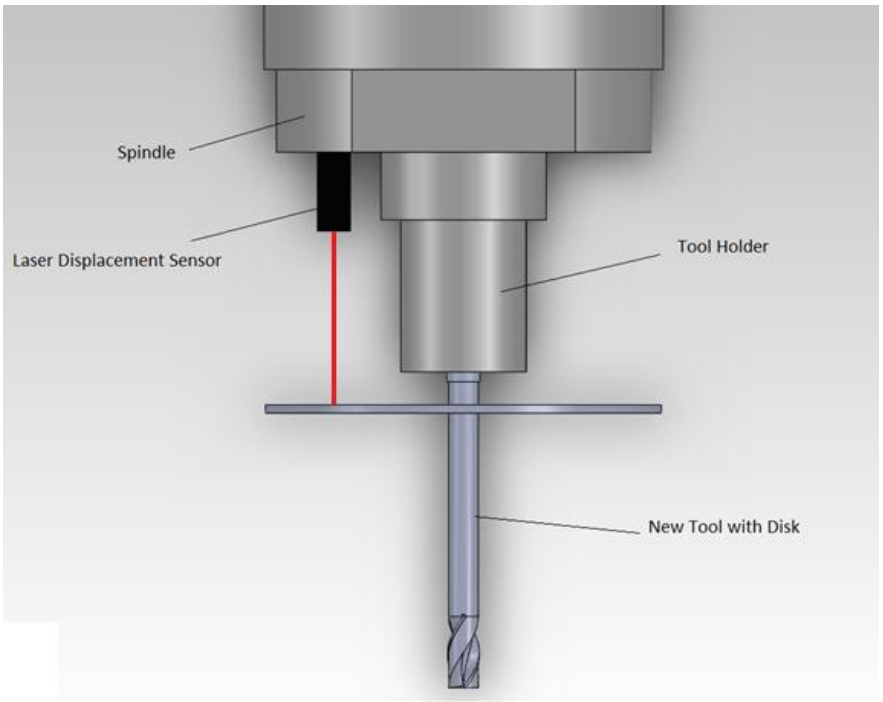

Figure 53: Ideal setup for future work using the thin disc attached to the cutting tool. A prototype of the new tool design will be manufactured so the thin disc is part of the cutting tool. A laser displacement sensor will replace the capacitance sensors allowing more freedom in the sensor location.

8.2: Modified New Cutting Tool Design

The broader range of measurement for the laser displacement sensor means the sensors have more freedom of positioning in the CNC machine. The laser displacement sensor isn't limited to being placed in an upright position (as seen in Figure 53) either. But the laser displacement sensors can't be placed at or below the height of the cutting tool due to potential interference with the workpiece.

The most advantageous way to utilize the laser displacement sensor is to measure the displacement of the cutting tool from above the cutting tool at an angle. Since the laser displacement sensor operates on the principle of triangulation, the thin disc must be modified to create a flat surface perpendicular to the laser [25]. To comply, the thin disc is replaced by an angled extrusion that encircles the cutting tool neck (see Figure 54). The angled extrusion can be solid or a thin shell design.

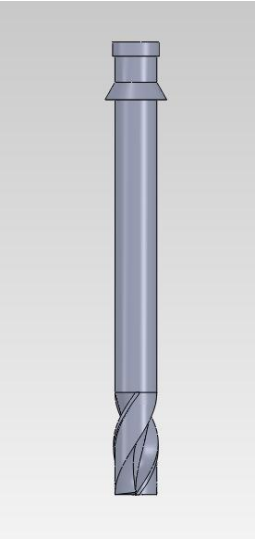

Figure 54: Modified new tool design has an angled extrusion circling the neck of the tool instead of the thin disc. The angled extrusion can be part of the cutting tool or an attachment placed on the neck of the cutting tool. The angled extrusion is a much smaller addition than the thin disc and would have less of an impact on the cutting tool mechanics.

The angled extrusion circling the neck of the tool can be an attachment or part of the cutting tool itself. The extrusion can be very small and angled at any position. The small size of the extrusion means that there will be less of an impact on the cutting tool mechanics compared to the new tool design with the large disc. The angle and height of the extrusion on the cutting tool neck must be oriented to create a clear path for the laser so as not to be obstructed by the workpiece or tool holder. The laser displacement sensors would be attached to the spindle on the x and y axis, and oriented to receive measurements from the angled extrusion circling the cutting tool (see Figure 55).

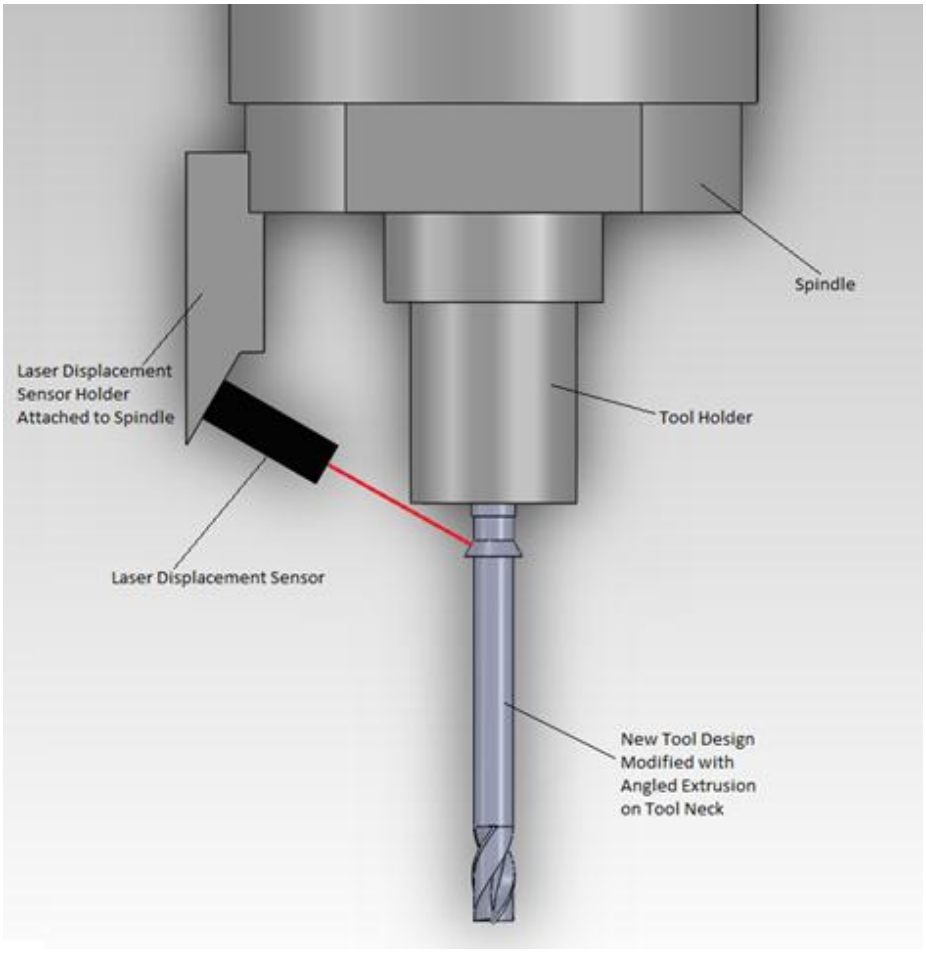

Figure 55: Possible setup for industrial use of the modified new tool design. The modified new tool design has an angled extrusion instead of the disc so the laser displacement sensor can measure the displacement at an angle.

8.3: Conclusion

In this research, a summary of the previous research conducted at the University of Missouri [13, 14] were summarized in (Chapters 1 and 2). A FEA was created to simulate the deflection of the cutting tool during chatter (Chapter 3). A new tool design was introduced that could potentially offer an alternate method to tool deflection and displacement measurement during milling operations (Chapter 4). A dynamometer was utilized to experimentally measure the difference in the cutting forces between the original cutting tool and the experimental new tool design (Chapter 5). The cutting forces found by the dynamometer and the tool displacements found by the prior tool displacement measurement method allowed for the verification of the Solidworks Simulation (Chapter 6). Once the FEA was verified, a simulation using the new tool design and experimental new tool design cutting forces was performed to simulate the new tool design during a milling operation (Chapter 6). Finally the experimental new tool design was utilized to perform tool displacement measurement experiments during milling operations (Chapter 7). The similarity between the results from the FEA method, experimental method and prior deflection measurement method (as seen in Figures 51 and 52) validates the feasibility of the new tool deflection measurement method.

While the addition of a small disc (Figure 10) or angled extrusion (Figure 54) on the cutting tool may be a small change to the tool design, the benefits in industry and research purposes are enormous. Tool displacements could be measured and monitored with little interference of sensors with this new tool design concept. Cutting fluid could be utilized since the laser displacement sensor can be placed away from the cutting area. And the laser displacement sensors run at a high frequency, so high speed milling can apply this new technique to eliminate chatter, the main obstacle in high speed milling.

Appendix

Appendix A: Dynamometer Calibration

For the calibration of the force in the x and y direction, a pulley system was aligned in the y direction of the CNC machine with one end of the cord tied to the cutting tool and the other end tied to a bucket. The pulley was propped up so that the cord was at a 90 degree angle with the cutting tool and so the bucket freely hung above the ground (See Figure 56). The bucket was found to weigh 9.786 Newton, and additional weights were placed in the bucket to apply tension in the cord which resulted in an applied force perpendicular to the cutting tool.

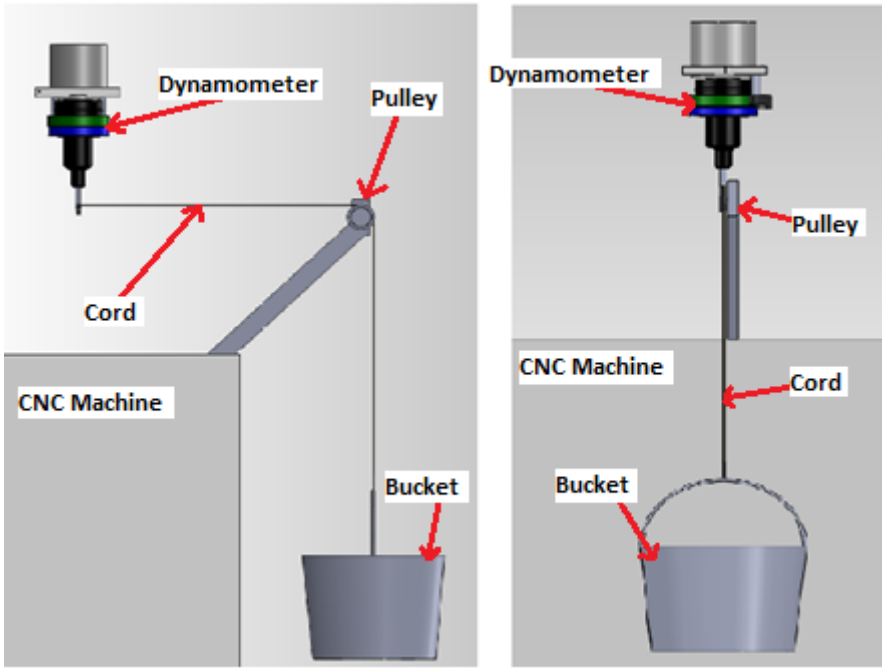

Figure 56: Side view of the dynamometer force calibration setup in the *x* and *y-direction* (left). Front view of the dynamometer force calibration setup in the *x* and *y-direction* (right).

To begin the dynamometer calibration of force in the x direction, the bucket was filled with all of the weights amounting to a force of 263.11 Newton. The large applied force outputted high voltage readings and made the forces in the x and y direction easier to observe.

The dynamometer was rotated until the voltage reading for the force in the y direction went to zero so that the force was applied only in the x direction. The dynamometer was locked in place and the weights were removed from the bucket. To obtain a calibration curve, the weights were placed in the bucket one at time and the voltage output from the dynamometer was recorded for each increment. The calibration constant for the dynamometer force sensor in the x-direction was found to be 5.53 mV/N (see Figure 57).

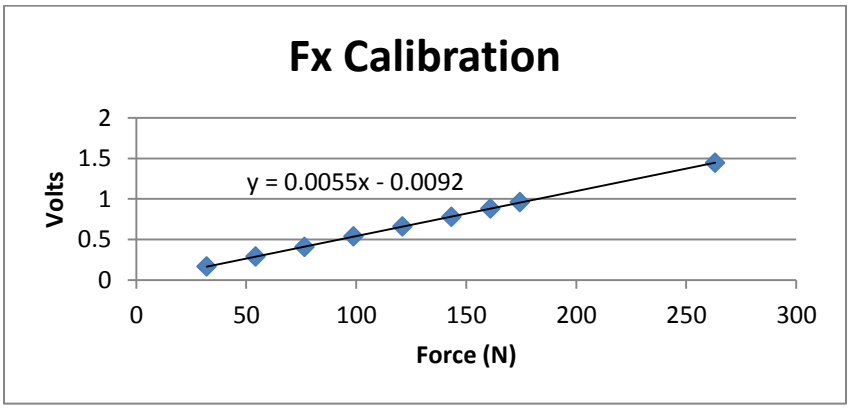

Figure 57: Calibration curve for the dynamometer force sensor in the x-direction.

To calibrate the dynamometer in the y direction, the same procedure was performed except the dynamometer was rotated until the voltage reading for the force in the x direction went to zero so the force was applied only in the y direction. The calibration constant for the dynamometer force sensor in the y direction was found to be 5.66 mV/N (see Figure 58).

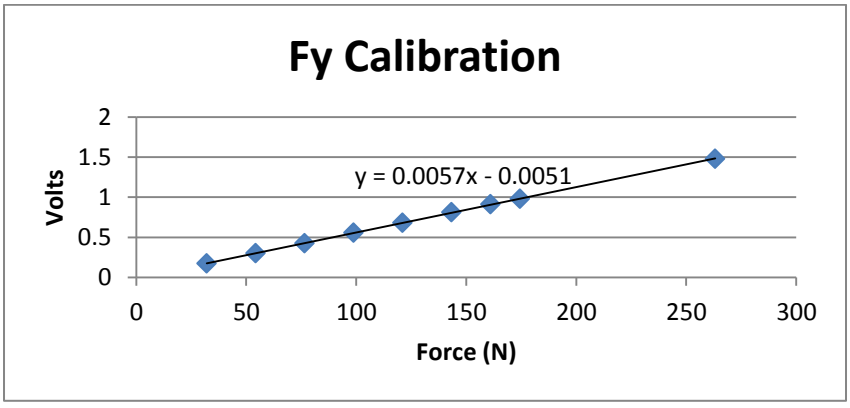

Figure 58: Calibration curve for the dynamometer force sensor in the x-direction.

To calibrate the dynamometer force sensor in the z-direction a see-saw contraption was assembled. The fulcrum of the see-saw contraption is directly placed in the center of the beam so that the force applied down on one end would be equivalent to the force applied up on the other. So one end of the see-saw was placed up against the bottom of the cutting tool, and the other end held the bucket containing the weights (see Figure 59).

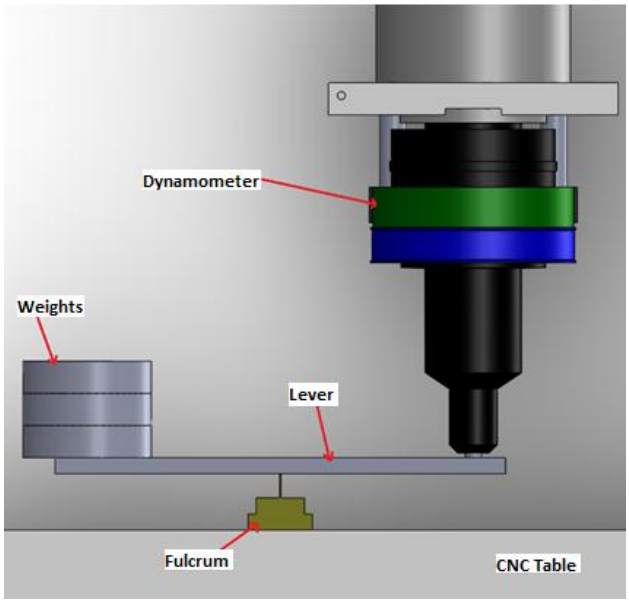

Figure 59: Front view of the dynamometer force calibration in the z-direction setup. Fulcrum of the lever is centered between the weights and the dynamometer so the force acting upward on the dynamometer is equivalent to the force acting downward from the weights.

The weights were placed in the on the see-saw in the same increments as the x and y direction calibration and the voltage output was recorded for each increment. The calibration constant for the dynamometer sensor in the z-direction was found to be 3.00 mV/N (see Figure 60).

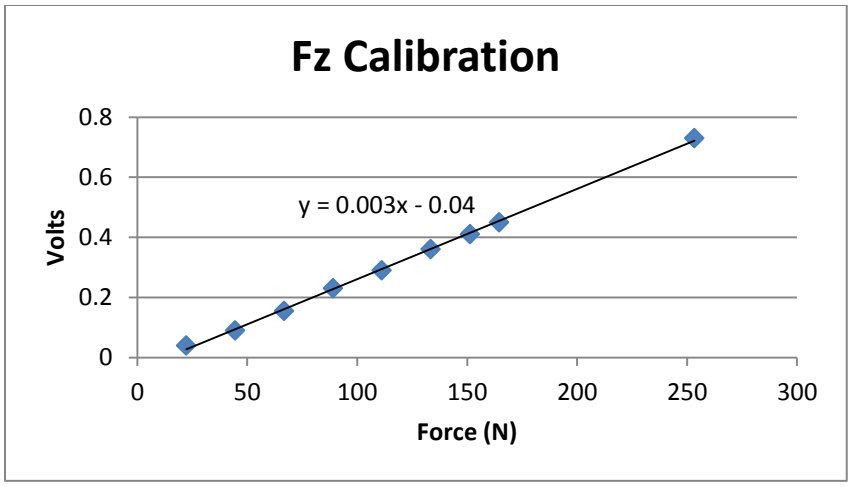

Figure 60: Calibration curve for the dynamometer force sensor in the z-direction.

To calibrate the clock-wise and counter clock-wise torque sensor of the dynamometer, a similar setup to the calibration of the force in the x and y direction was utilized. A moment arm was constructed with two cylinders extruding from one surface of a metal rectangle with a distance of 0.3048 m from center to center of the two cylinders (see Figure 61).

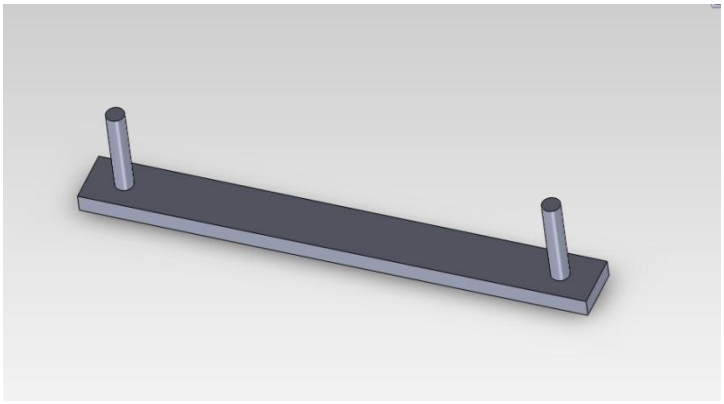

Figure 61: Moment arm that was used in the dynamometer calibration for torque in the clock-wise and counter clock-wise direction. The cylinders are 0.3048 m from center to center and the diameter of the cylinders is 0.5 in. to match the diameter of the cutting tool.

To start the calibration, the dynamometer was locked into place using the spindle orient command to keep the dynamometer from rotating. Then one cylinder of the moment

arm was placed in the tool holder of the dynamometer and tightened in oriented so the moment arm was aligned with the x-axis. For torque in the counter clock-wise direction, the pulley system was shifted -0.3048 m in the x-direction, and the cord was tied to the other cylinder to create a 90 degree angle with the moment arm. For torque in the clock-wise direction, the moment arm was rotated 180 degrees. The pulley system was shifted 0.3048 m in the x-direction, and the cord was tied to the other cylinder to create a 90 degree angle with the moment arm (see Figure 62).

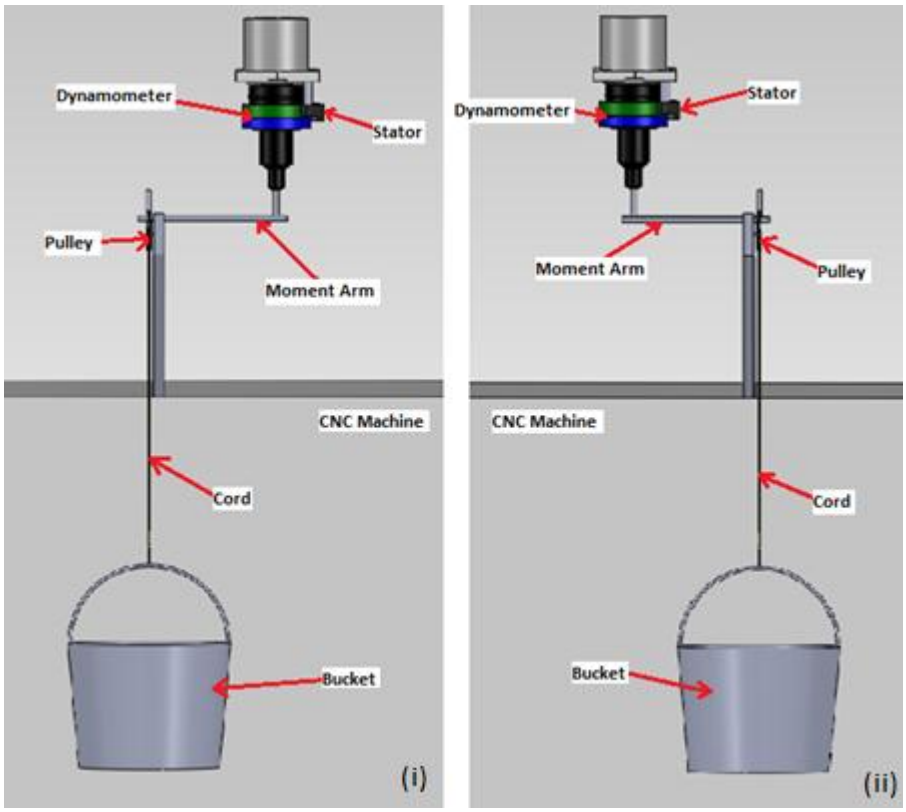

Figure 62: Front view of the dynamometer torque calibration in the (i) counter-clockwise direction and (ii) clockwise direction.

For both the counter clock-wise and clock-wise direction torque setups, the weights were placed in the bucket to create incremental torque and the voltage output from the dynamometer was recorded at each torque. The calibration constant for torque in the clock-

wise direction was found to be 87.1 mv/Nm, and the calibration constant for torque in the clock-wise direction was found to be -88.6 mV/Nm (see Figure 63)

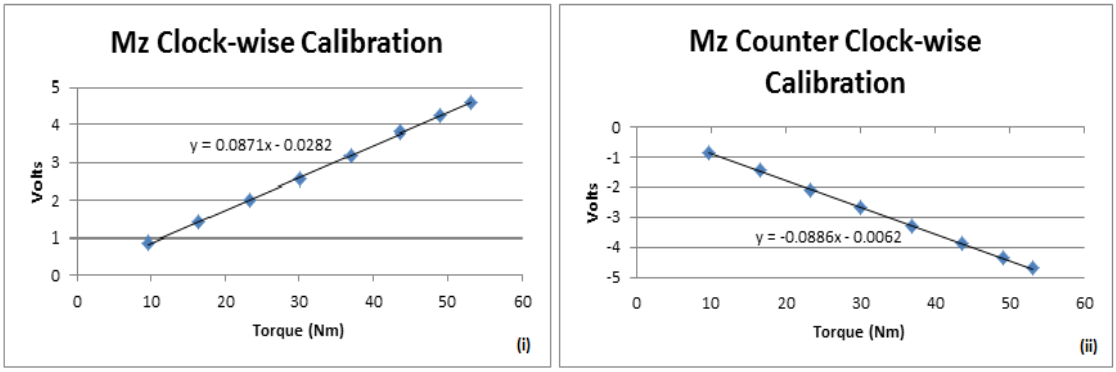

Figure 63: Dynamometer calibration curve for torque in the clock-wise direction (i). Dynamometer calibration curve for torque in the counter clock-wise direction (ii).

Appendix B: Capacitive Sensors Calibration

Since the CNC machine has a built in positioning system accurate to 1/10000 of an inch, it became a helpful tool in the calibration process of the capacitive sensors and made the calibration relatively easy. The capacitive sensors were securely mounted on the CNC table and positioned so that it is aligned with the x-direction of the CNC machine and so the cutting tool shaft can be used as the measured object (see Figure 64). The capacitive sensor and the cutting tool shaft are initially touching. The cutting tool remains stationary while the CNC table is moved in the positive x direction in increments of 0.0762 mm. At each increment the voltage from the capacitive sensor is recorded and this process is repeated until the distance between the capacitive sensors reaches 1 mm. The results are then plotted and a calibration curve is determined by a best fit first polynomial line (see Figure 65). This entire process was repeated

for the second capacitive sensor. The calibration constants were found to be 10.1874 V/mm for the first capacitive sensor and 10.9206 V/mm for the second capacitive sensor.

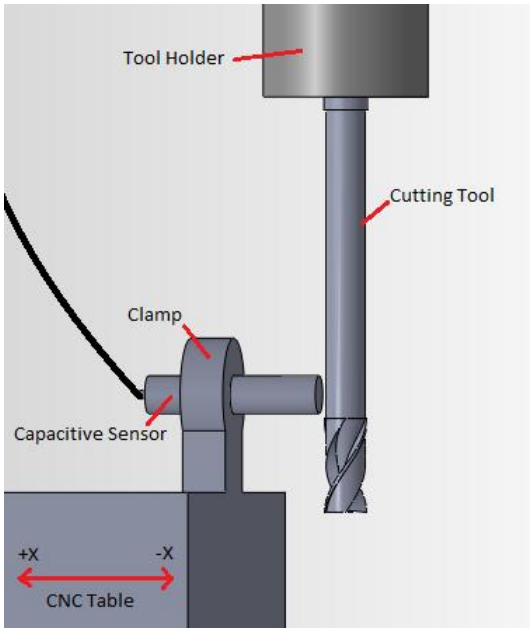

Figure 64: Calibration Setup for the capacitive sensors. The capacitive sensors were aligned in the x-direction so the CNC hand wheel could easily give a known distance to the 1/10000 of an inch.

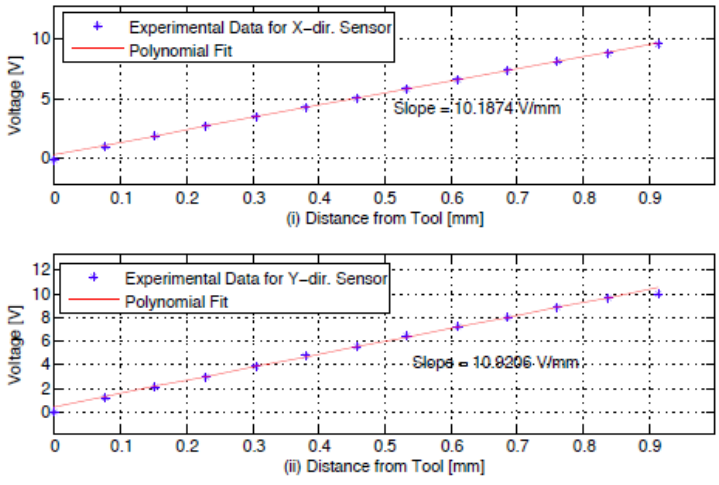

Figure 65: Calibration curves for the capacitive sensors. (i) x-direction sensor. (ii) y-direction sensor.

References

[1] M. C. Shaw, “Metal Cutting Principles,” Oxford: Oxford University Press, Inc., 1997.

[2] J. Tlusty, “Manufacturing Processes and Equipment,” Upper Saddle River, NJ: Prentice Hall, 1 ed., 2000.

[3] Sigmund Max Young, “Dynamics of Low Immersion Milling,” 2008

[4] B. Jabbaripoor, A Habibzadeh, and M. H. Sadeghi, “Cutting Force Modeling in End-Milling Operation of Titanium Thin Walled Parts,” 2009

[5] P. V. Bayly, and B. P. Mann, "Effect of Radial Emersion and Cutting Direction on Chatter Instability in End-Milling," ASME International Engineering Congress & Exposition, Nov. 2002.

[6] J. Tlusty, Manufacturing Processes and Equipment, 1 ed. Upper Saddle River, NJ: Prentice Hall, 2000.

[7] M. H. Kurdi, T. L. Schmitz, R. T. Haftka, and B. P. Mann, "Simultaneous Optimization of Removal Rate and Part Accuracy in High-Speed Milling," in Proceedings of ASME International Mechanical Engineering Congress and Exposition, IMECE04, Anaheim, CA, 2004.

[8] B. P. Mann, N. K. Gary, K. A. Young, and A. M. Helvey, "Milling Bifurcations from Structural Asymmetry and Nonlinear Regeneration," Nonlinear Dynamics, vol. 42, pp. 319-337, 2005.

[9] E. Budak, and Y. Altintas, "Analytical Prediction of Chatter Stability in Milling – Part 1: General Formulation," Journal of Dynamic Systems, Measurement, and Control, vol. 120, pp. 22-30, 1998.

[10] M. A. Davies and B. Balachandran, “Impact Dynamics in Milling of Thin Walled Structures,” 2000

[11] Y. Atlintas, “Manufacturing Automation,” 1st edition, 2000

[12] F. W. Taylor, "On the Art of Cutting Metal," in Transactions of ASME, 1907

[13] Joseph Kennedy, “Chatter Detection and Prevention in High-Speed Milling,” PhD Dissertation, Mechanical and Aerospace Engineering, University of Missouri, Columbia, 2011.

[14] A. Radhakrishnan, "Effect of Chip Thickness, Sub-Critical Bifurcations and

Process Parameters in High-Speed Milling," PhD Dissertation, Mechanical and Aerospace Engineering, University of Missouri, Columbia, Columbia, MO, 2010.

[15] Kistler, “Operating Instructions: Rotating Cutting Force Dynamometer,” 1997

[16] H. Toriya, H. Chiyokura, “3D CAD: Principle and Applications,” 1993

[17] Wang Zhao, “Force Analysis and Process Optimization of End Milling,” 1991, pp. 37-41

[18] H. Toriya, H. Chiyokura, “3D CAD: Principles and Applications,” 1993

[19] S. Smith, and T. Delio, "Sensor-Based Control for Chatter-Free Milling by Spindle Speed Selection," in Proceedings of the ASME 1989 Winter Annual Meeting, 1989, pp. 107-114.

[20] Raymond F. Neathery, “Statics and Applied Strength of Materials,” 1985

[21] Alfred Jensen, and Harry Chenoweth, “Statics and Strength of Materials,”4th edition, University of Washington, Seattle.

[22] Y. Atlintas and E. Budak, “Analytical Prediction of Stability Lobes in Milling,” CIRP Annals, 1995.

[23] M.A. Davies, J.R. Pratt, B. Dutterer, And T.J. Burns, “Interupted Machining: A Doubling in the Number of Stability Lobes,” Journal of Manufacturing Science and Engineering, 2003.

[24] James F Shackelford, William Alexander, Jun S. Park, “CRC: Materials Science and Engineering,” CRC Press, Inc, 1994, pg. 508

[25] H. X. Song, X. D. Wang, L. Q. Ma, M. Z. Cai, T. Z. Cao, “Design and Performance Analysis of Laser Displacement Sensor Based on Position Sensitive Detector,” Journal of Physics: Conference Series 48 (2006) pg. 217-222.